NASA Technical Memorandum 83254

A Calibration Technique for a Hot-Wire-Probe Vector Anemometer

James Scheiman, Charles Marple,
and David S. Vann

MARCH 1982

NASA

NASA Technical Memorandum 83254

A Calibration Technique for a Hot-Wire-Probe Vector Anemometer

James Scheiman, Charles Marple,
and David S. Vann
Langley Research Center
Hampton, Virginia

National Aeronautics
and Space Administration

**Scientific and Technical
Information Branch**

1982

SUMMARY

Calibration tests using hot wires were conducted using a newly developed test rig that greatly reduced the data-acquisition time. The tests included a three-wire probe and a single-wire probe operating at numerous speeds and flow angles. A comparison of measured and computed velocity-vector magnitude and direction indicates the necessity of complete probe calibration to determine flow interference and/or operating limitation regions. Calibration results indicate that flow rates with 3-percent accuracy and flow angles with 5° accuracy are attainable.

INTRODUCTION

Flow situations often arise where there is a requirement for making dynamic velocity-vector measurements. When the velocity varies in magnitude and direction at a fairly rapid rate, only a few types of sensors can be used to make the measurements. Small scale models are often used which impose size limitations on the sensor in order to avoid the problem of flow interference by the sensor itself.

Examples of this type dynamic environment are flow regions downstream of a propeller or a helicopter rotor and within a tip vortex. The velocity vector near the plane of the blades changes both in magnitude and in direction with each blade passage. For some operating conditions the velocity vector can completely reverse direction. Because of the relatively rapid blade passage, the velocity sensor should have a fairly high-frequency response. Also, all three velocity components are desired. In order to gain a better understanding of the rotating-blade dynamic loads and to correlate with available theories, blade-generated acoustics (specifically tip-vortex impulsive blade noise) and measured dynamic velocity distributions are essential.

A few methods are available for making dynamic velocity measurements. These are a laser Doppler velocimeter system, a hot-wire vector system, and a hot-film system. The laser Doppler velocimeter (LDV) has the advantage of not introducing any flow disturbance into the flow stream. However, this system is very costly compared with the hot-wire systems, and an LDV system requires a relatively long development time to become operational. For the propeller or helicopter rotor example cited, the LDV system measures particle motion through a small sensing volume, and the corresponding measurements are not continuous as with a hot-wire or hot-film sensor (i.e., the LDV averages particle motion over a large number of blade passages). The hot-wire system has the disadvantage of introducing a sensor into flow streams that are being measured and thus creating a flow interference which may disturb the flow being measured. In addition, flow disturbances can occur because of the hot-wire prongs (wire supports). The required three velocity components necessitate three hot wires, and the corresponding sensor volume is larger than the sensor volume for an LDV system. The sensor volume can be important because the sensor detects the average velocity within that volume. Thus, if the velocity gradients within the volume are too great, errors are introduced. Advantages of the hot-wire system are that it is relatively cheap to purchase, requires very little development time, and has a fairly high-frequency response. A hot-film system has advantages and disadvantages similar to a hot-wire system, and it is much less vulnerable to damage.

When using a hot-wire system, the questions of "accuracy" and "flow-angle limitations" immediately come to mind. The user of a three-hot-wire system often provides very little calibration information (e.g., refs. 1 to 3). There are several reasons for this lack of calibration data. A complete-probe calibration involves testing at numerous velocities and directions; thus, a complete calibration is very difficult to obtain. Further, the physical endurance of the three-hot-wire system can become a serious limitation if the calibration becomes too extensive and requires a large amount of operating test time. Because of these problems, the hot-wire probe user in many cases cannot or does not calibrate the probe. Instead, the user relies on analytical data-reduction equations, and in some cases uses published sensor sensitivities. Such an approach neglects probe or hot-wire support-prong flow interference and any estimate of accuracy for determining velocity magnitude or direction. Also, slight differences between probes because of fabrication tolerances are neglected. The importance of some of these effects can be found, for example, in references 4 to 11. When the flow is nearly parallel to the longitudinal axis of one of the hot wires, or when hot-wire support-prong interference is encountered, system inaccuracies should be anticipated. Therefore, there are flow angles where the measured results should be questioned even though the measurements may be repeatable. Some attempts have been made to estimate accuracy and probe operating limitations.

The subject of this paper is a limited calibration and a discussion of some operating problems when using hot wires to make mean velocity-vector measurements. Recommended procedures were used to reduce the data, and the resulting computed velocity magnitudes and directions are compared with the corresponding measured values. A special calibration rig was developed and used to shorten the data-acquisition time. This reduction was achieved by taking advantage of the rapid response time of the hot wire and by making use of electronic data reduction techniques. This calibration rig is described herein. Two three-wire probes and one one-wire probe were tested. The hot-wire output data were reduced at 5° increments in flow angle with respect to the probe axis, over a range of ±155°. These data were obtained at various probe roll angles. The flow velocities varied from 8.94 to 40.23 m/s.

SYMBOLS

A constant determined by calibration (see eq. (1)), $\text{volts}^2/°\text{C}$

a constant determined by calibration (see eq. (2)), $\left(\frac{\text{kg}}{\text{m}^2\text{-s}}\right)^{1/2}$

B constant determined by calibration (see eq. (1)), $\text{volts}^2/°\text{C}\left(\frac{\text{m}^2\text{-s}}{\text{kg}}\right)^{1/2}$

b constant determined by calibration (see eq. (2)), $\left(\frac{\text{kg}}{\text{m}^2\text{-s-volts}^4}\right)^{1/2}$.

c constant determined from the intercept of a least-squares-fit line through measured and computed mass flow (see eq. (4)), $\left(\frac{\text{kg}}{\text{m}^2\text{-s}}\right)^2$

d constant determined from slope of a least-squares-fit line through measured and computed mass flow (see eq. (4)), dimensionless

E dc voltage supplied to wire sensor, volts

K constant in equation (3), dimensionless

n constant ranging from 0.48 to 0.51, $n = 1/2$ herein

T_e temperature of environmental cooling fluid, °C

T_s temperature of hot-wire sensor, °C

U total velocity-vector magnitude, m/s

V velocity component normal to hot wire, m/s

θ acute angle between flow direction and longitudinal axis of hot wire, deg

ρ density of cooling fluid, kg/m^3

ϕ probe roll angle measured from vertical plane through probe axis to hot wire 1, deg

ψ probe yaw angle with respect to flow direction (0 when velocity is aligned with probe axis), deg

Subscripts:

e experimental calibrated angle

g geometrical angle

i ith hot wire ($i = 1, 2, 3$) for three-wire probe

m minimum

θ denotes quantity at a particular value of θ

APPARATUS AND TEST PROCEDURE

Apparatus

Hot-wire system.- Three hot-wire probe systems were tested in this study. The prongs of all the probes were gold plated. The wires were platinum-plated tungsten with an active wire diameter of 5 μm and an active length of 1.25 mm (length-to-diameter ratio of 250). The total hot-wire length (distance between prongs) was 3 mm, which is about three times the active wire length. The probes were operated in a constant-temperature mode and no linearizer was used. The wires were operated at an overheat ratio of 1.8, which is within the recommended operating range.

Two of the probes were typical three-wire probes of identical manufacture. These probes have three wires, each of which is perpendicular to the other two. Looking along the axis of the probe, the hot wires project an image onto a normal

plane of 120° between wires. Figure 1(a) is a photograph of one of these probes. Disregarding flow interferences, this probe system could theoretically measure the magnitude and direction of the velocity anywhere in a hemisphere.

The third probe had a single wire. Figure 1(b) is a photograph of this probe. This type probe construction is designed to minimize flow interference for some test conditions.

Calibration rig.- A complete calibration of a three-hot-wire probe over a speed range requires many test conditions (thousands in this report) and can be very time consuming. In order to decrease the time, a special calibration rig has been constructed. This calibration rig makes use of the rapid response time of a hot-wire system and greatly reduces the testing time. Figure 2 is a photograph of this rig. The hot-wire probe shown on the calibration rig in figure 2 can be yawed about a point near the center of the hot wires. The maximum yaw-angle range was about ±170° (data were recorded over a range of ±155°), and the yawing rate could be varied from about 6 to 20 seconds per cycle. During the high-speed tests, the aerodynamic drag on the probe support arm was such that the yaw rate was relatively slow against the wind and relatively fast with the wind. In fact, the maximum torque of the yaw motor was the factor that limited the maximum tunnel test speed. However, even at the yaw-rate extremes, the crank-arm tangential velocity was small compared with the flow velocity. The structural deflection of the system was insignificant.

Figure 2 also shows the square-wave yaw-angle position indicator. This indicator consisted of a saw tooth and a photocell which generated an electrical square wave over a range of ±155° at intervals corresponding to every 5° of yaw for the probe systems. The calibration of the probe yaw angle and square-wave generator is shown in table 1. The saw-tooth gear was machined very accurately; however, the orientation of the zero-yaw position (probe angle with respect to the free stream) was not good (as seen by the uneven angles in table 1). This resulted in fixed angular displacement for all the yaw angles. A "flip-flop" system was incorporated in order to indicate the probe yawing direction of rotation (i.e., clockwise or counterclockwise). The hot-wire probe system could be manually oriented at different roll angles about the probe axis. An optical system (transit theodolite) was used to adjust the roll angle of the hot wires on the calibration rig.

Test Procedure

The tests were conducted in the low-velocity calibration wind tunnel at the Langley Research Center. A photograph of this tunnel is shown in figure 3. The tunnel test chamber is 43.2 cm wide, 30.5 cm high, and 76 cm long, and the speed range is from 2.2 to 89.4 m/s. The turbulence level in the test chamber is about 0.5 to 0.75 percent, which is adequate for the measurements presented in this report. The tunnel velocity can be measured to 0.5-percent accuracy. The fluid temperature was the ambient temperature and was constant within the measuring accuracy.

As the calibration rig cycled back and forth through the yawing cycles, the electrical outputs were recorded continuously and simultaneously on different channels of an FM magnetic-tape recorder. These electrical outputs consisted of the three hot-wire voltages, the square-wave-yaw identification pulse, and the direction-of-yaw flip-flop indicator. In addition, the probe identification, probe roll orientation, probe yawing rate, and tunnel speed were manually recorded. Two extreme yawing rates, about 6 and 20 seconds per cycle, were used. For the current tests,

the tunnel speed varied from 8.9 to 40 m/s in intervals of about 4.5 m/s for a total of seven speeds. As viewed along the axis of the probe, roll angles ϕ of 0° and 90° were chosen for the three-wire probes (first with number one hot wire vertical and second with number one hot wire horizontal). Looking along the axis of the three-wire probe, the projection of the three wires in a normal plane are 120° apart. The single-wire probe was also tested over the same speed range and at the same roll angles ϕ of 0° and 90° (i.e., the single wire vertical and horizontal). Using the previously described procedures, the total data-acquisition time was reduced to a few hours. The hot-wire, yaw-angle-pulse, and direction-of-rotation outputs were recorded simultaneously on a magnetic-tape recorder. At least 40 complete yaw cycles of the probe were recorded for each operating test condition. The recorded data were reduced as follows. The magnetic-tape data were digitized at the appropriate rise and fall positions indicated by the square-wave yaw-angle signal. (When the probe is yawing in one direction, the probe yaw angle for the rise on the square wave corresponds to the same probe yaw angle for the fall on the square wave when yawing in the opposite direction.) Infrequently during the recording of the square-wave generator signal, a noise spike or reduced level was recorded. This would be detected during the digitizing process of one complete probe yaw cycle, because one square-wave pulse would be added or omitted. Therefore, before any single complete cycle of data was processed further, the total number of digitized data points for each probe yaw cycle was counted. If the sum did not add up to 62, all the data within that cycle were discarded. When the data for one yaw cycle were accepted, the hot-wire voltages corresponding to each probe yaw position were squared (to obtain electrical power when wire resistance was assumed constant). These values were accumulated for all the complete cycles and were then averaged. The data for the different directions of yawing rotation were averaged separately so that the effects, if any, of the direction of yaw could be evaluated. The final output (voltage squared) values presented herein represent at least 40 averaged data points for each probe yaw position. The mean output (voltage squared) values and standard deviations were tabulated and machine plotted. The standard deviations were calculated in order to evaluate the scatter in the data.

DISCUSSION OF RESULTS

Three hot-wire probes were tested in the low-velocity calibration wind tunnel at the Langley Research Center. The probes were tested at seven speeds and yaw angles over a range of ±155° to determine interference and other deviations from theory. The results are presented in four sections: (1) probe geometric limitations, (2) probe response with yaw, (3) comparison of two identical three-wire probes, and (4) velocity magnitude (mean flow) and direction prediction.

Probe Geometric Limitations

When using a three-wire probe, three operating problem regions are considered: (1) when one hot wire is downstream of another wire, (2) when the velocity vector is parallel to the axis of a wire, and (3) when there is flow interference due to the wire supports (prongs). The first two operating regions are discussed in this section, and these operating limits are called probe geometric limits herein. The third region requires a complete calibration and is discussed herein. When the mean velocity vector is known, the problem of geometric limits can be minimized by proper orientation of the probe with respect to the flow direction. However, when the mean velocity vector is not known, there is no way of orienting the probe to avoid the operating problem regions. Instead, it is essential to make measurements at two or

more probe orientations, reduce the data, and compare the results for similarity. If the results for any two probe orientations are not similar, there is no way of knowing which measurement, if either, is correct, and a third (or more) measurement is required.

The probe geometric limits discussed in this section are associated with flow at some fixed angle to the axis of a hot wire θ. In order to maintain accuracy, the probe operation should be limited to an operating region where the flow angle θ is not small. Generally, for a three-wire probe, the individual wires are aligned perpendicular to each other. This orientation simplifies the mathematics in determining the total flow rate from the output of the three wires (e.g., section 7.3C of ref. 12). From the wire geometry and the known flow angle ψ with respect to the probe axis, the angle θ between the velocity vector and any wire axis can be determined. These computational procedures are given in the appendix, and the graphical results are shown in figure 4.

The center of the polar plot in figure 4 shows the orientation of the three hot wires as seen looking along the axis of the probe. The polar angle ϕ (roll angle) on the figure represents the direction of the velocity vector component in a plane normal to the axis of the probe. The yaw angle ψ, graduated along a radial line in the figure, represents the angle between the velocity vector and probe axis. Thus, any point on the plot specifies the angular position of the velocity vector with respect to the probe (center of plot). The advertised hemispherical limit to probe operation would be indicated in the figure by a circle with a radius equal to $\psi = 90°$. The contour lines are for $\theta_m = 20°$, $30°$, and $40°$. This angle θ_m is defined as the angle between the velocity vector and the (longitudinal) axis of any hot wire. The figure also shows the orientation of the velocity vector with respect to the fixed probe.

The area between the circle for $\psi = 0°$ and any θ_m curve defines the probe operating region where θ for any of the three hot wires will always be greater than θ_m. The plot shows that, for the solid line, the ψ angles (between the velocity vector and probe axis) must not be greater than about 16°. Further, for the $\theta_m = \geqslant 30°$ boundary, ψ can be as large as 23°, and for the $\theta_m \geqslant 20°$ boundary, ψ can be 36°. In other words, if the velocity-vector orientation is unknown, and if $\theta_m \geqslant 20°$ is considered a reasonable minimum value (refs. 2 and 5), then the angle between the hot-wire probe axis and the velocity vector must be less than about 36°. This represents a physical limit for probe operation.

Probe Response With Yaw

The data presented herein are well beyond the manufacturer's recommended yaw angles of usability (i.e., greater than hemisphere) for this sensor. However, since this is an exploratory program, the complete range of measured data is presented. Initially, the probe data recorded when approaching a given yaw angle from upstream and downstream were accumulated and averaged separately. This procedure provided an evaluation of the effect of yawing direction on the results. A comparison between average probe output when approaching a given yaw angle from upstream or downstream proved the differences were negligible. Thereafter, the data at each yaw angle for both directions of yawing were averaged together. Thus, the mean values of the output (volts squared) in figures 5 to 9 are averages of at least 80 individual test points for each of the 62 probe yaw angles.

A standard deviation was calculated for each test condition. The standard deviation provides a measure of scatter in the individual data and also an evaluation of the variation of the mean value or the number of individual data points required to decrease the variation in the mean value. It was initially believed that absolute scatter in the data would be highest at probe yaw angles with flow interference on one of the hot wires (i.e., θ small). However, this was not usually the case. The reason for the variation in the scatter with θ could not be determined.

The one standard deviation value σ varied from 0.5 percent to 2 percent of the mean value of the output. Letting one standard deviation equal 2 percent, two standard deviations, which include 95 percent of the data, are within ±4 percent of the mean value. In other words, one test point would have ±4-percent accuracy with a 95-percent confidence. Averaged data presented herein, which are average values $\bar{x}$ of about 80 individual points, are accurate to within ±0.5 percent with a confidence of 95 percent $\left(\sigma_{\bar{x}} = 0.04/\sqrt{80}\right)$.

The bottom plots of figures 5(a) to 5(c) are plots of the output against the probe position or yaw angle for each of the three wires or sensors of the probe. Lines are faired through the discrete data points. The symbols on the curves are only used to identify the various mean flow rates (each faired curve includes data at every 5° of yaw angle). The top plots of figures 5(a) to 5(c) show the calculated flow angle θ with respect to that wire. (When $\theta = 90°$, the velocity is perpendicular to the axis of the wire.) The different curves in the bottom plots of figures 5(a) to 5(c) are for different mass flow ρV. Figures 5(a), 5(b), and 5(c) are for wires 1, 2, and 3, respectively, of the probe. The wires are numbered consecutively in a clockwise direction when looking from the rear of the probe. In figure 5, the number one wire was aligned vertically. The figure shows that maximum hot-wire output (cooling) occurs when the fluid flow is perpendicular to the wire ($\theta = 90°$). Discontinuities in the output (cooling rate or volts supplied) curves are indications of flow interference. For example, for wire number one in figure 5(a) there is flow interference for a probe yaw angle of about 75°. Figure 5 also shows that some of the interferences are velocity dependent rather than geometry dependent. When the interference occurs at all mass flow rates at the same yaw angle ψ it is primarily a geometric interference (e.g., fig. 5(b), $\psi = 100°$). When the interference occurs at different mass flow rates, it is velocity dependent (e.g., fig. 5(b), $\psi = -24°$ or 26°). As mentioned previously, the output data presented are accurate to ±0.5 percent of mean value with a confidence limit of 95 percent; therefore, the noted effect cannot be attributed to errors in data acquisition.

For the lowest mass flow ($\rho V = 10.89$), there are two curves. These two curves were obtained by cycling the calibration rig at yaw rates of 6 and 20 seconds per cycle. It was expected that the largest difference induced by the cycling rate would occur at the lowest flow rate. As seen in the figure, the curves for the two cycling rates are nearly identical. Therefore, it is concluded that for the lowest mass flow tested, the cycling rate or yawing velocity had very little effect on wire output.

Figure 5 also shows two curves for a mass flow rate ρV of 21.81. These two curves were obtained from data taken on different days. Differences in these curves provide an indication of calibration repeatability and wire deterioration with usage. Figure 5(b) for wire 2 indicates some unexplainable shift in the mean value. The other two sensors on the probe do indicate some differences, but they are relatively small (≈0.5 percent).

For any one curve in figure 5, the mass flow rate is constant; therefore, the output (wire cooling or power supplied) is directly related to flow angle θ with respect to each wire. (When θ is highest, the cooling is highest; when θ is lowest, the cooling is lowest.) The larger the variation in θ with probe yaw, the larger the variation in output (volts squared). The variation in θ was calculated from the known geometry of each sensor on the probe and the measured probe yaw position.

The data presented in figure 6 follow the same format as the data presented in figure 5. The figure 6 data are for the same probe; however wire 1 is horizontal (looking from the rear, wire 1 is to the left). In figure 5 wire 1 was vertical. Figure 6(a) shows that there is a linear relationship between θ and ψ, as would be expected. Also, because of probe symmetry, wires 2 and 3 should and do have identical geometrical characteristics with variation in yaw angle.

Figure 6 shows many of the same characteristics already seen in figure 5. For example, some of the cooling interferences are slightly velocity dependent (fig. 6(a), $\psi = 75°$) and some interferences are geometric (fig. 6(b), $\psi = -133°$, or fig. 6(c), $\psi = -123°$). The output (volts squared) curves show that the geometric interferences for wires 2 and 3 around $\psi = -123°$ are not the same. This may be because the wires are symmetrical and the sensor support prongs are not.

The variation in output is a function of the variation in the flow angle θ with respect to each wire. In general, figure 6 shows that the same wire with equal values of θ but with different values of ψ can have different cooling rates. This is indicative of the differences in flow interference over the extreme yaw-angle range. For example, in figure 6(a) for $\rho V = 15.13$, the maximum output values for $\theta = 90°$ (at $\psi = -143°$ and $35°$) are not equal. Likewise, for the same wire and the same ρV, the minimum output values are unequal for $\theta = 0°$ at $\psi = -54°$ and $120°$. Further indications of flow interference are shown by comparing the calculated yaw angles for minimum cooling ($\theta = 0°$) with the measured values. For example, in figure 6(a) the calculated yaw angles for minimum cooling are $-52.7°$ and $127.7°$, whereas the measured minimum cooling is at about $\psi = -48°$ and $130°$. This same effect can be seen in other data (e.g., fig. 7(c)). This implies that the probe yaw angles ψ should be restricted to perhaps $\pm 50°$ to $\pm 70°$. Also, the angular flow limitations described in figure 4, which are based on probe geometry, may be too restrictive.

Figure 7 presents the response characteristics of a second three-wire probe identical to the probe used to obtain the data presented in figures 5 and 6. This probe had wire 1 aligned vertically; therefore the data can be compared directly with the data in figure 5. The results are similar for the two probes.

In addition to the three-wire probes, the single-wire probe shown in figure 1(b) was tested on the calibration rig. Figure 8(a) shows the response for this probe with the wire aligned vertically, and figure 8(b) shows the response with the wire aligned horizontally. In figure 8(a), the mass flow direction is always at 90° to the wire (the sensor is yawed about its axis as the calibration rig cycles in yaw). Figure 8(a) shows that the output (cooling rate) is nearly constant (within 1 percent) as the yaw varies. There is severe interference by the wire-prong supports at one of the extreme yaw positions ($\psi = 111°$) and not at the other. This would be expected from the physical construction of this type probe.

In figure 8(b), where the single wire is oriented horizontally, the mass flow angle θ varies linearly with the probe yaw angle. Note the symmetry in the output (cooling rate), even for the points of minimum cooling at $\psi = \pm 85°$ and $\pm 90°$. The

data in figure 8 for the single-wire probe indicate a lack of interferences (as expected). This fact is illustrated by the smoothness of the curves with variations in either mass flow rate or yaw angle.

Comparison of Two Similar Three-Wire Probes

A comparison of the response of the two three-wire probes which are of identical model and manufacture is presented in figure 9. The data presented in figure 9 were obtained by offsetting the mean voltage levels by the same amount for all three wires on one probe. This was done to obtain a relative comparison for the two probes. The slopes of these curves indicate the capability of determining flow direction from the three curves for any one sensor. Since the slopes for each wire on the two probes are about the same, there is a strong similarity in the individual wires of the two probes.

The major flow interferences seem to occur at the same probe yaw angles. Most noticeable is the larger number of interferences for probe 1 as compared with probe 2. These differences are most probably due to the hot-wire—prong joint connection differences on a very small scale. This seems apparent for all three wires on probe 1, especially for wire 2. Although these differences are on the order of only a few percent, they underscore the need for calibrating each individual probe through a range of velocities and yaw and roll angles if accuracy is to be attained. This calibration should be extensive enough to obtain data-reduction constants and an assessment of the interference for each probe. Unfortunately, any single probe may not last long enough to perform the calibration (as is the case herein with probe 1, which failed during calibration).

Velocity Magnitude and Direction Prediction

Throughout this report the discussion has been associated with mass flow rate ρV rather than velocity. There are a number of equivalent ways to describe these terms. For example, when the density is known, the mass flow can be converted directly to velocity. Another common procedure is to convert the actual mass flow rate to that of standard-density mass flow rate. With this understanding the mass flow rate and velocity terms are used interchangeably herein.

To evaluate the capability of determining the magnitude of the velocity from the three-wire probe, the following procedure is normally used. From equation (1) of reference 12 (where the mass flow is perpendicular to the wire sensor, i.e., $\theta = 90°$),

$$E^2 = \left[A + B(\rho V)^{1/2}\right](T_s - T_e) \tag{1}$$

By solving equation (1) for the mass flow rate ρV and recalling that for constant-temperature operation T_s is constant (for the current test T_e is sufficiently constant that $T_s - T_e$ can be considered constant), equation (1) can be rewritten as

$$(\rho V)^{1/2} = bE^2 + a \tag{2}$$

where the constants a and b are determined from the data tabulated for the tests herein. Since one probe was tested with wire 1 in two positions (figs. 5 and 6), the a and b constants were determined separately for both series of tests. As recommended by the manufacturer, each wire on the probe should be calibrated with the mass flow at 90° to the wire ($\theta = 90°$). Data at some probe yaw positions were discarded because flow interference was present. (See figs. 5 and 6.) After specifying a particular probe yaw position (near $\theta = 90°$) for each wire, all the ρV data and the corresponding E^2 experimental data were accumulated and a least-squares-fit straight line through the data was determined. The constants a and b correspond to the intercept and slope of the least-squares-fit line. Table 2 summarizes the results. In table 2 there are four values of the a and b constants for each wire on the probe. Normally, the calibration procedure is to determine only one value for each wire. For any of the three wires, the differences between the constants are small for the same probe roll position (as indicated by horizontal or vertical position of wire 1). There is a relatively large difference between the constants for the same wire when the probe roll positions are different. This variation for the a and b constants, especially for wires 2 and 3, could be attributed to deterioration of the individual wires with usage. The first series of tests were conducted with the probe roll angle such that wire 1 was vertical (fig. 5). This series of tests required about 3 hours of wind-tunnel air blowing across the probe. While conducting the second series of tests (with the probe roll angle such that wire 1 was horizontal), wires 2 and 3 failed. The implication is that the wire endurance is not sufficient to last through a complete calibration. The wires were operating at acceptable temperature limits; however, small particles may have struck these two wires on the probe.

Velocity magnitude calibration.- To continue the evaluation of the mass flow prediction accuracy, the two values for the constants a and b determined with wire 1 vertical, which were almost the same, were averaged together. The mass flow rates determined from each of the three wires can be combined into a total mass flow by using the following equation from section 7.3C of reference 12:

$$(\rho U)^2 = \frac{(\rho V_1)^2 + (\rho V_2)^2 + (\rho V_3)^2}{2 + K^2} \tag{3}$$

During the derivation of this equation, it is assumed that the values of K for each wire are all equal and that the individual wires are perpendicular to each other.

For one probe yaw angle (fig. 5) and the a and b constants for each wire and the output (volts squared) for each wire, $(\rho V_i)^2$ could be determined by using equation (2). The numerator of the right-hand side of equation (3) could then be calculated. This calculated value could then be compared with the actual measured mass flow rate (left-hand side of eq. (3)). These results are shown in figure 10 for various probe yaw angles. Also shown in figure 10 are least-squares-fit straight lines through the data which are represented by

$$(\rho U)^2 = d \sum_{i=1}^{3} (\rho V_i)^2 + c \tag{4}$$

where c and d are constants. The c and d constants are tabulated in table 3, which shows that the constant c (the intercept for the straight lines in fig. 10) is small as would be expected. This shows that the computed mass flow from the individual wire output is nearly zero when the actual flow is zero. The correlation in figure 10 neglected the denominator on the right-hand side of equation (3), $(2 + K^2)$. This value corresponds to the value of d determined from the least-squares-fit straight line. Solving for K^2 from $d = 1/(2 + K^2)$ results in negative values for K^2, which is contrary to recommended values (e.g., ref. 13). Using the recommended value of K^2 as 0.02 results in $d = 1/(2 + K^2) = 0.495$. Comparing this value with the d value in table 3, it can be seen that the capability of using the probe for predicting the mass flow rate is good if the predicted (hot-wire) values are within 3 percent of the measured values. The same a and b constants used in the above correlation, which is based on data from figure 5, were used to predict the flow rates for the probe tests with wire 1 horizontal (as for fig. 6). As might be expected from the previous discussion of probe deterioration, the correlation of the computed and actual flow rates was poor. When a and b constants determined from tests with wire 1 horizontal were used (see table 2), the correlation did not improve appreciably.

Velocity direction calibration.- For an evaluation of the use of the three-wire probe to predict the flow direction, the following procedure was used. The flow-direction determination with respect to the probe is dependent upon the capability of determining the flow angle θ with respect to the individual wires. From the sine-law relationship in reference 12, it can be determined that

$$\frac{(\rho V_\theta)^2}{(\rho V_{\theta=90^\circ})^2} = \sin^2 \theta + K^2(\cos^2 \theta) \tag{5}$$

or using equation (2), equation (5) can be rewritten as

$$\left[\frac{\left(bE_\theta^2 + a\right)}{\left(bE_{\theta=90^\circ}^2 + a\right)}\right]^4 = \sin^2 \theta + K^2(\cos^2 \theta) \tag{6}$$

This function represents the relationship between the maximum mass flow cooling rate ($\rho V_{\theta=90^\circ}$) and the mass flow cooling rate when the fluid is moving at some angle θ with respect to the individual wire. Equation (6) can be used to solve for the flow angle θ with respect to one of the wires for any measured output (volts squared), once the constant K and the maximum cooling rate ($\rho V_{\theta=90^\circ}$) have been determined. The constant K is a function of flow rate (ρV or V) and was determined herein as a function of flow rate. Constants a and b for each wire have already been determined and are known to provide good results for predicting the mass flow rate for the probe described in figure 5 and table 2. From figure 5, two probe yaw angles were chosen that were known to be free of interference; one yaw angle corresponds to the maximum cooling ($\theta = 90^\circ$) and the other yaw angle corresponds to near-minimum cooling. From the measured output at these two probe yaw angles and with the known a and b constants, $(\rho V)^2$ and $(\rho V_{\theta=90^\circ})^2$ were determined. These quantities were in turn used with the known wire flow angle θ and equation (6) to determine the constant K. The constant K was determined for both the maximum and minimum mass flow rates for each wire, and the squares of these values are tabulated in

table 4. As stated previously, with K known, equation (6) was used to compute the flow angle θ with respect to each wire from the measured wire output (volts squared) at numerous probe yaw angles (fig. 5). From the top portion of figures 5(a) to 5(c), the geometric flow angle θ was also determined for the same probe yaw angle. The resulting comparison of the computed geometric angles and the flow angles from application of the calibration data and calculated from equation (6) are shown in figure 11.

Figures 11(a), 11(b), and 11(c) present the correlation for each of the three wires on the probe. These data correspond to the probe response data shown in figure 5, where wire 1 was aligned vertically. The correlation for the maximum and minimum flow rates are both shown in figure 11. The data presented include probe yawing in both directions. Also, data are included for probe operation well beyond its operating limits, namely with yaw angles greater than 90° (flagged symbols) or flow from the rear of the probe. The solid symbols are data points from figure 5 that are suspected of involving probe flow interference. Figure 11 also shows the ideal correlation line. While equation (6) is simple to use and is recommended by the manufacturers, to obtain more accurate results a complete calibration with a varying K value or more complex equation should be used (e.g., see refs. 7, 8, 9, 10, and 14).

Figure 11(a), which is for wire 1, includes flow angles θ from 55° to 90°, which correspond to the θ values in figure 5(a). The data in figure 11(a) show good correlation, with only a few data points showing an error greater than 5°. The two data points in figure 11(a) where flow interference is suspected (solid symbols) show relatively poor correlation. Without some knowledge of flow interference or probe limitations, probe operation in this region would result in poor accuracy. Note the large negative values of K^2 for wire 1 in table 4. Of course, these values of K^2 do not appreciably affect the correlation. This is because of the relatively large values of θ. For example, from equation (6), with $\theta > 55°$ as in figure 11(a), the $\sin^2 \theta$ term is dominant compared with the $K^2 \cdot \cos^2 \theta$ term.

Figure 11(b) is for wire 2 and corresponds to the data in figure 5(b). Figure 11(b) shows fair correlation at relatively low flow angles, $25° < \theta < 35°$, and poor correlation at large flow angles, $60° < \theta < 80°$. The poor correlation in the vicinity of $\theta = 90°$ is not understood because the same values of a and b were successfully predicted in the mass flow in figure 10. The correlation in figure 11(b) shows flow-angle errors up to 20°.

Figure 11(c) presents the correlation for wire 3 on the probe and corresponds to the response data in figure 5(c). The data for probe operation with suspected flow interference and for extreme probe yaw angles do not seem to affect the correlation. In general, the correlation indicates that the flow angles for this sensor can be predicted within 5°, which is considered good.

It is concluded that for the three-wire probe tested herein, for probe flow angles ϕ less than 30°, and with adequate probe calibration, the mass flow rate can be predicted within a few percent (fig. 10). However, with inadequate probe calibration, the flow angles may have errors as large as 20°. Furthermore, without a complete probe calibration, errors of at least this magnitude should be expected. With the flow angle determined with respect to each wire, the total velocity vector is completely defined in space, and this vector can be resolved into any desired coordinate system.

To complete the flow-angle calibration study, the single-wire probe with the wire in the horizontal position was evaluated. The correlation is shown in figure 12 which was determined from the sensor response data shown in figure 8(b). With the single wire horizontal, the probe yaw angle is equal to the mass flow angle ϕ with respect to the wire. Correlation for the maximum and minimum flow rates are shown. The data presented include probe yaw angles in both directions. The data in figure 12 show that the flow-angle values predicted from the sensor response are almost all lower than the ideal values. An error in the determination of K^2 would have a more pronounced effect on the correlation errors for the smaller values of θ and would have little effect at the larger values of θ. From equation (5) for θ approaching 90°, the $\sin^2 \theta$ approaches 1 and the $K^2 \cdot \cos^2 \theta$ approaches 0, whereas for θ approaching 0°, the $\sin^2 \theta$ approaches 0 and the $K^2 \cdot \cos^2 \theta$ approaches K^2. Therefore, the resulting correlation errors shown in figure 12 must be attributed to the determination of $(\rho V/\rho V_{\theta=90°})^2$ in equation (5). If a minimum of correlation data had been recorded to determine the appropriate data-reduction constants, the flow angle determined with a single-wire probe would be approximately 5° in error.

CONCLUDING REMARKS

Hot-wire calibration tests were conducted with a newly developed test rig. This procedure consists of the recording of the analog hot-wire output along with a square-wave-generator signal as the probe cycles continuously through a range of flow angles. The data are then electronically digitized and analyzed at intervals dictated by the square-wave generator. The test rig utilized was effective in acquiring and processing a large amount of data in a relatively short period of time.

A comparison of two probes of identical model and manufacture indicated some differences in response and flow interference. A statistical analysis of the scatter in the individual data points (volts) indicates a scatter of about ±4 percent. As shown by increasing the number of points averaged, the scatter of the mean values can be reduced to approximately ±1 percent with a 95-percent-confidence limit.

Flow interference is one major contributor of error in using a three-wire probe without an extensive calibration or without severely limiting the operation of the probe. Because of the limited endurance of the probe, it is strongly recommended that precalibrations and postcalibrations be performed even when the calibration is curtailed. When a comparison of the two calibrations do not agree, the data should not be used. With precalibrations and postcalibrations and operation flow-angle limits with respect to the axis of the probe of 30°, 3-percent accuracy in determining mass flow rates was attained. Furthermore, with only limited probe calibration, flow-angle errors of 20° were observed. However, with extensive calibrations, these flow-angle errors can be decreased to 5°.

Langley Research Center
National Aeronautics and Space Administration
Hampton, VA 23665
January 28, 1982

APPENDIX

EQUATIONS FOR COMPUTING HOT-WIRE GEOMETRIC FLOW ANGLES

The equations derived in this appendix are used to determine the acute angle θ between the velocity vector and the longitudinal axis of each of the hot wires. When $\theta = 0$, the velocity is parallel to the wire axis. The numerical results from applying these equations are shown graphically in figure 4. For these derivations, the subscripts c and s are used to designate the trigonometric cosine and sine of the associated angle (i.e., $\theta_c = \cos\theta$, $\phi_s = \sin\phi$). A Cartesian coordinate system fixed to the probe is aligned with the $\vec{k}$-axis along the probe stem. Furthermore, let the vectors $\overrightarrow{HW1}$, $\overrightarrow{HW2}$, and $\overrightarrow{HW3}$ be defined as being parallel to hot wires 1, 2, and 3, respectively. Hot wire 1 lies in the i-k plane as shown in the sketch which follows:

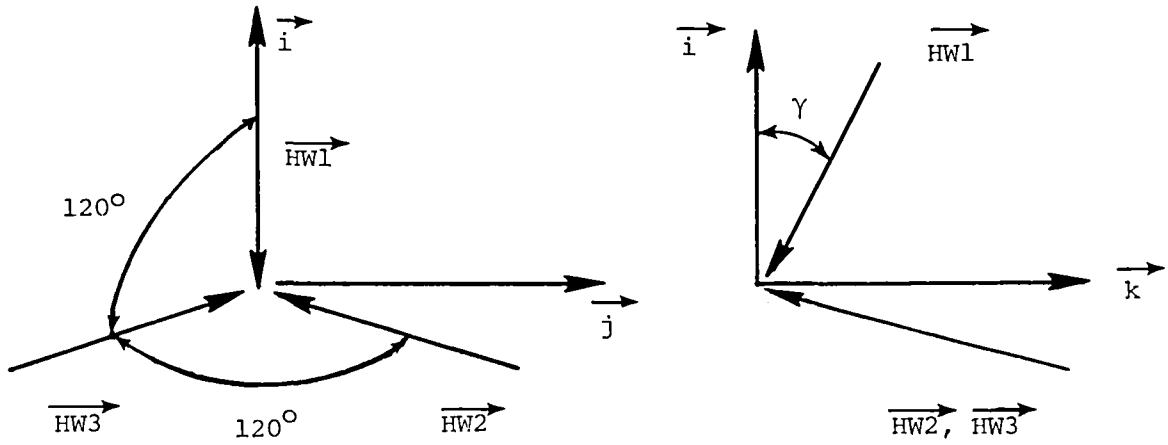

The angle γ that the vectors $\overrightarrow{HW1}$, $\overrightarrow{HW2}$, and $\overrightarrow{HW3}$ make with the i-j plane was set by the manufacturer as 35.26°, so that $\gamma_s = 1/\sqrt{3}$ and $\gamma_c = \sqrt{2/3}$. The vectors $\overrightarrow{HW1}$, $\overrightarrow{HW2}$, and $\overrightarrow{HW3}$ are related to the Cartesian system by

$$\begin{Bmatrix} HW1 \\ HW2 \\ HW3 \end{Bmatrix} = \begin{bmatrix} -\gamma_c & 0 & -\gamma_s \\ \frac{1}{2}\gamma_c & -\gamma_c\frac{\sqrt{3}}{2} & -\gamma_s \\ \frac{1}{2}\gamma_c & \gamma_c\frac{\sqrt{3}}{2} & -\gamma_s \end{bmatrix} \begin{Bmatrix} i \\ j \\ k \end{Bmatrix}$$

where i, j, and k are orthogonal unit vectors.

APPENDIX

An unknown velocity vector $\vec{V}$ can be resolved into components with respect to the probe coordinate system by determining the roll angle ϕ and yaw angle ψ shown in the sketch which follows:

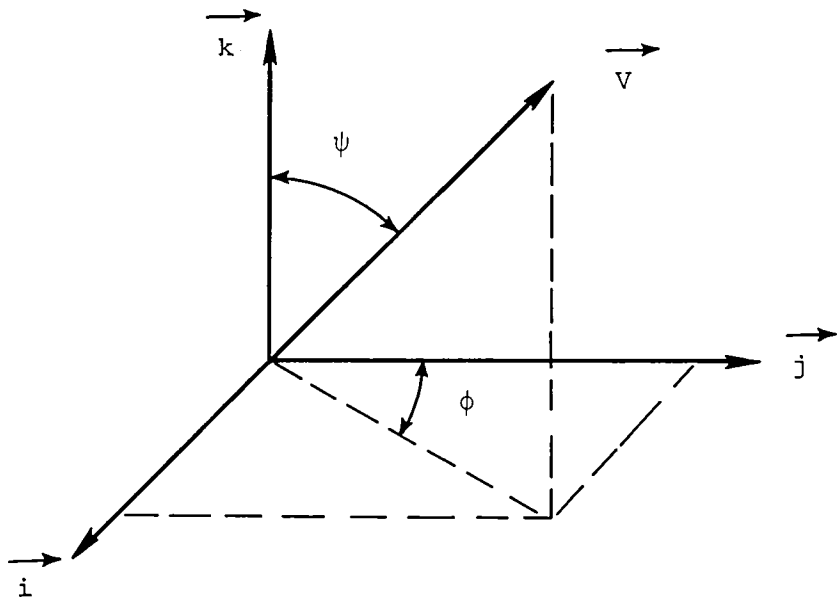

$$\begin{Bmatrix} V_i \\ V_j \\ V_k \end{Bmatrix} = \begin{Bmatrix} \psi_s \phi_s V \\ \psi_s \phi_c V \\ \psi_c V \end{Bmatrix} \tag{A1}$$

Since only the angle between a hot wire and the velocity vector is desired, the magnitude of the velocity vector is set equal to one ($|V| = 1$). The tangent of θ is equal to the component of the velocity perpendicular to the wire divided by the component parallel to the wire. The vector dot product of $\vec{V}$ and $\overrightarrow{HW}$ results in the velocity component parallel to the wire, and the corresponding vector cross product results in the velocity perpendicular to the wire. The magnitude of the cross product is the square root of the sum of the square of each component. Therefore, for HW1

$$\tan \theta_{HW1} = \frac{\vec{V} \times \overrightarrow{HW1}}{\vec{V} \cdot \overrightarrow{HW1}} = \frac{\left[\left(\frac{1}{3} + \frac{2}{3}\phi_c^2\right)\psi_s^2 + \frac{2}{3}\psi_c^2 - \frac{2\sqrt{2}}{3}\phi_s\psi_s\psi_c\right]^{1/2}}{-\frac{\psi_c}{\sqrt{3}} - \sqrt{\frac{2}{3}}\psi_s\phi_s} \tag{A2}$$

and for HW2 and HW3

$$\tan \theta_{HW2} = \frac{\left[\left(\frac{1}{3} + \frac{\phi_c^2}{6} + \frac{\phi_s^2}{2} + \frac{\phi_s\phi_c}{\sqrt{3}}\right)\psi_s^2 + \frac{2}{3}\psi_c^2 + \left(-\frac{2}{\sqrt{6}}\phi_c + \frac{2}{\sqrt{18}}\phi_s\right)\psi_s\psi_c\right]^{1/2}}{\left(\frac{\phi_s}{\sqrt{6}} - \frac{\phi_c}{\sqrt{2}}\right)\psi_s - \frac{\psi_c}{\sqrt{3}}} \tag{A3}$$

$$\tan \theta_{HW3} = \frac{\left[\left(\frac{1}{3} + \frac{\phi_c^2}{6} + \frac{\phi_s^2}{2} - \frac{\phi_s\phi_c}{\sqrt{3}}\right)\psi_s^2 + \frac{2}{3}\psi_c^2 + \left(\frac{2}{\sqrt{6}}\phi_c + \frac{2}{\sqrt{18}}\phi_s\right)\psi_s\psi_c\right]^{1/2}}{\left(\frac{\phi_s}{\sqrt{2}} + \frac{\phi_s}{\sqrt{6}}\right)\psi_s - \frac{\psi_c}{\sqrt{3}}} \tag{A4}$$

By choosing various combinations of the probe roll angle ϕ and yaw angle ψ, these equations can be solved for θ_{HW1}, θ_{HW2}, and θ_{HW3}. The results of the numerical solution are presented in figure 4.

REFERENCES

1. Rorke, James B.; and Moffitt, Robert C.: Wind Tunnel Simulation of Full Scale Vortices. NASA CR-2180, 1973.

2. Jacobsen, Robert A.: Hot-Wire Anemometry for In-Flight Measurement of Aircraft Wake Vortices. Advancements in Flight Test Engineering, Fifth Annual Symposium Proceedings, Soc. Flight Test Eng., c.1974, pp. 4-13 - 4-24.

3. Corsiglia, Victor R.; Jacobsen, Robert A.; and Chigier, Norman: An Experimental Investigation of Trailing Vortices Behind a Wing With a Vortex Dissipator. NASA paper presented at the Symposium on Aircraft Wake Turbulence (Seattle, Wash.), Sept. 1970.

4. Zalay, Andrew D.; White, Richard P.; and Balcerak, John C.: Investigation of Viscous Line Vortices With and Without the Injection of Core Turbulence. Rep. 74-01 (Contract No. N00014-71-C-0226), Rochester Appl. Sci. Assoc., Inc., Feb. 1974. (Available from DTIC as AD 785 256.)

5. Yavuzkurt, Savas; Crawford, Michael E.; and Moffat, Robert J.: Real-Time Hot-Wire Measurements in Three-Dimensional Flows. Symposium on Turbulence, G. K. Patterson and J. L. Zakin, eds., Science Press, c.1979, pp. 265-279.

6. Larsen, Sören E.; Mathiassen, Olaf; and Busch, Niels E.: Analysis of Data From 3-Dimensional Hot-Wire Probes Using Comparison With Profile Instrumentation for Calibration. Proceedings of the Dynamic Flow Conference 1978 on Dynamic Measurements in Unsteady Flows, c.1978, pp. 591-597.

7. Champagne, F. H.; Sleicher, C. A.; and Wehrmann, O. H.: Turbulence Measurements With Inclined Hot-Wires. Pt. 1. Heat Transfer Experiments With Inclined Hot-Wire. J. Fluid Mech., vol. 28, pt. 1, Apr. 12, 1967, pp. 153-175.

8. Gilmore, D. C.: The Probe Interference Effect of Hot Wire Anemometers. TN. 67-3 (D. R. B. Grant No. 9551-12), McGill Univ. (Montreal), July 1967.

9. Friehe, C. A.; and Schwarz, W. H.: Deviations From the Cosine Law for Yawed Cylindrical Anemometer Sensors. Trans. ASME, Ser. E: J. Appl. Mech., vol. 35, no. 4, Dec. 1968, pp. 655-662.

10. Kjellström, Björn; and Hedberg, Stellan: Calibration Experiments With a DISA Hot-Wire Anemometer. AE-338, Aktiebolaget Atomenergi (Stockholm, Sweden), Nov. 1968.

11. Collis, D. C.; and Williams, M. J.: Two-Dimensional Convection From Heated Wires at Low Reynolds Numbers. J. Fluid Mech., vol. 6, pt. 3, Oct. 1959, pp. 357-384.

12. Hot Film and Hot Wire Anemometry - Theory and Application. Bull. TB5, Thermo-Systems, Inc.

13. Webster, C. A. G.: A Note on the Sensitivity to Yaw of a Hot-Wire Anemometer. J. Fluid Mech., vol. 13, pt. 2, June 1962, pp. 307-312.

14. Delleur, Jacques W.: Flow Direction Measurement by Hot-Wire Anemometry. J. Eng. Mech. Div., American Soc. Civil Eng., vol. 92, no. EM4, Aug. 1966, pp. 45-70.

TABLE 1.- PROBE YAW POSITION CALIBRATION

Probe position number[1]	Probe yaw angle[2]
0	-148°40'
5	-123°40'
10	-98°40'
15	-73°40'
20	-48°40'
25	-23°40'
30	1°20'
35	26°20'
40	51°20'
45	76°20'
50	101°20'
55	126°20'
60	151°20'
61	156°20'

[1]Each probe position number represents a 5° yaw angle increment.

[2]Positive yaw angles represent flow from left of probe axis when looking upstream.

TABLE 2.- CONSTANTS FOR USE WITH EQUATION (2)

Probe roll position	Probe yaw angle, deg	a	b	θ, deg
Wire 1				
Wire 1 vertical	-98.7 -88.7	-0.2738 -.2575	0.7216 .7044	85.0 90.7
Wire 1 horizontal	26.3 41.3	-0.2470 -.2464	0.7384 .7275	81.1 83.9
Wire 2				
Wire 1 vertical	-43.7 -38.7	-0.1611 -.1707	0.4608 .4601	81.4 89.5
Wire 1 horizontal	-58.7 121.3	-0.2448 -.2581	0.6892 .6878	87.2 87.2
Wire 3				
Wire 1 vertical	31.3 41.3	-0.2206 -.2235	0.6678 .6675	82.8 88.1
Wire 1 horizontal	-63.7 -53.7	-0.3081 -.3029	0.8092 .8031	83.7 89.2

TABLE 3.- CONSTANTS FOR USE WITH EQUATION (4)

ψ, deg	d	c
0	0.4993	0.00158
10	.5173	.00121
-10	.5022	.00149
20	.5164	.00134
-20	.5040	.000904
30	.4980	.00129
-30	.4752	.00133

TABLE 4.- CONSTANTS FOR USE WITH EQUATION (6)

Probe/sensor	ρV, kg/m^2-s	K^2
Three-wire probe, wire 1 vertical; wire 1	43.82 10.89	-0.4034 -.7244
Three-wire probe; wire 1 vertical; wire 2	43.82 10.89	0.1471 .1536
Three-wire probe; wire 1 vertical; wire 3	43.82 10.89	-0.02485 -.04879
Single-wire sensor Single-wire sensor	43.30 10.82	0.00330 .00499

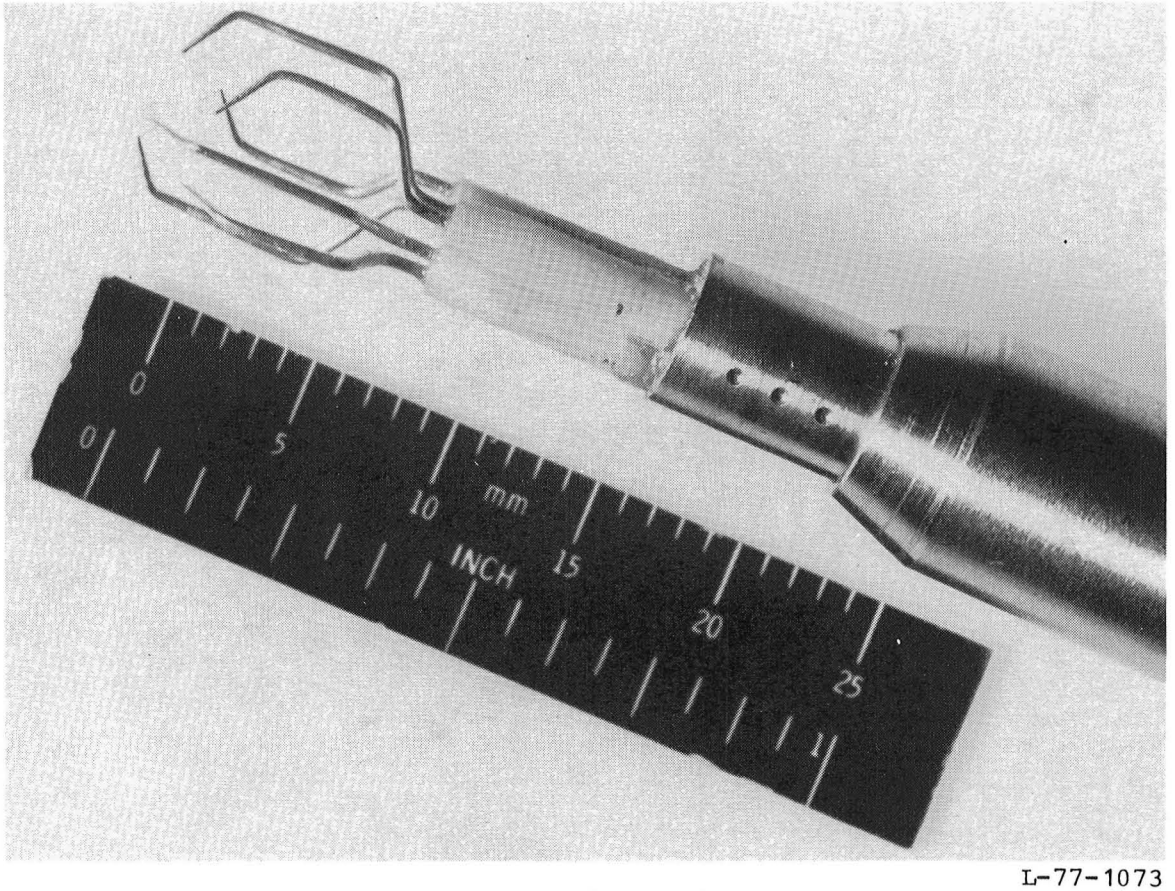

L-77-1073

(a) Three-wire probe.

Figure 1.- Two types of hot-wire probes tested.

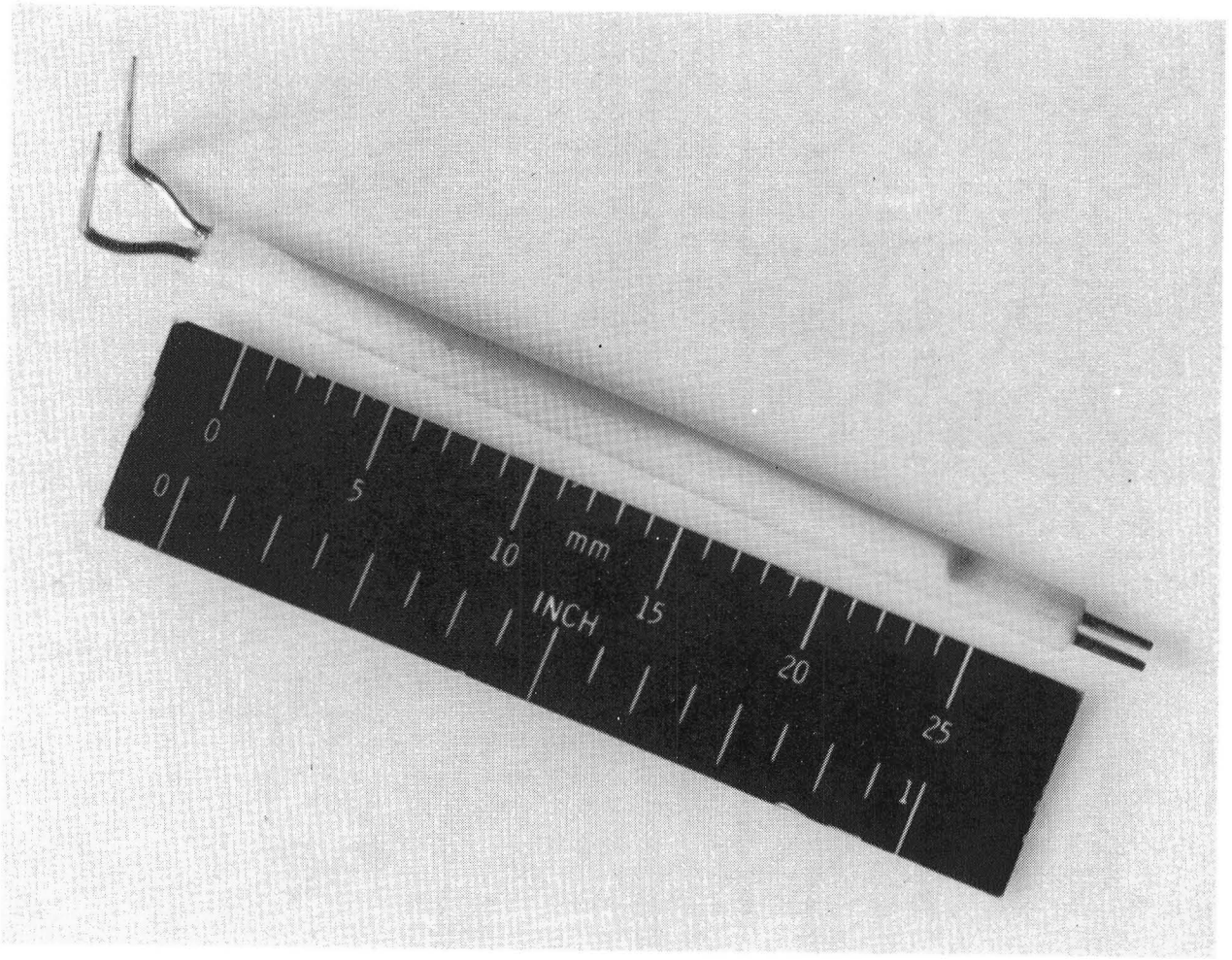

L-77-1070

(b) Single-wire probe.

Figure 1.- Concluded.

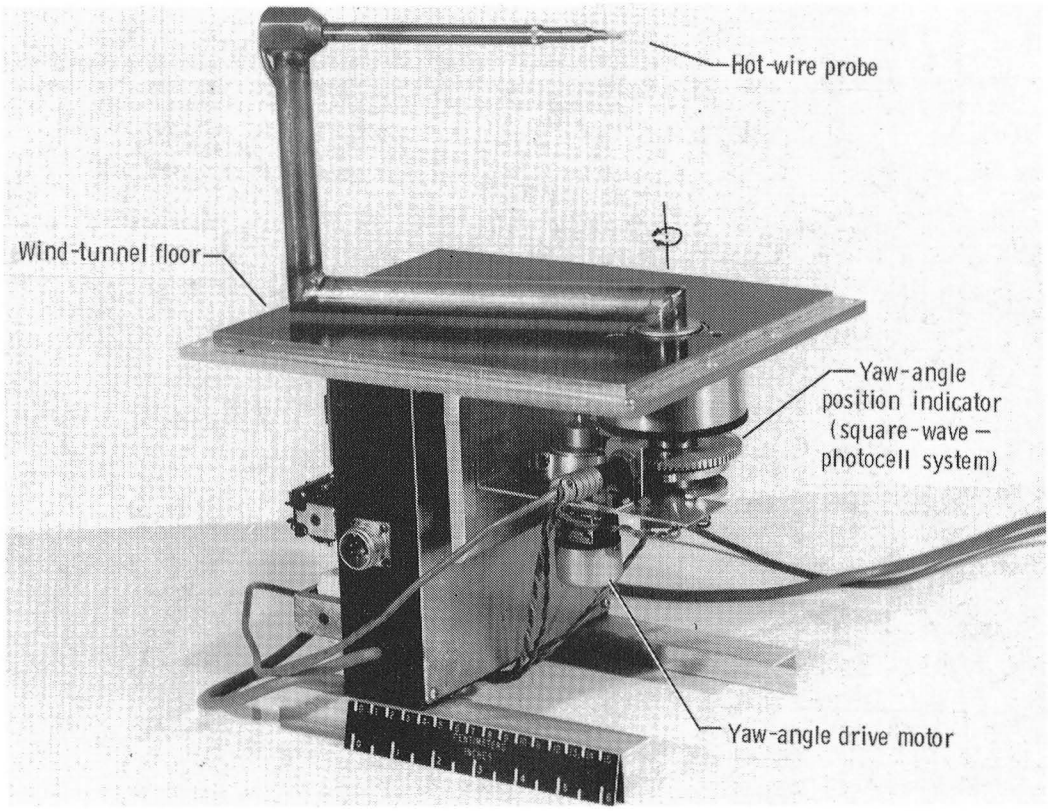

L-77-1069.1

Figure 2.- Hot-wire calibration rig.

L-76-1321.1

Figure 3.- Low-velocity calibration wind tunnel at the Langley Research Center.

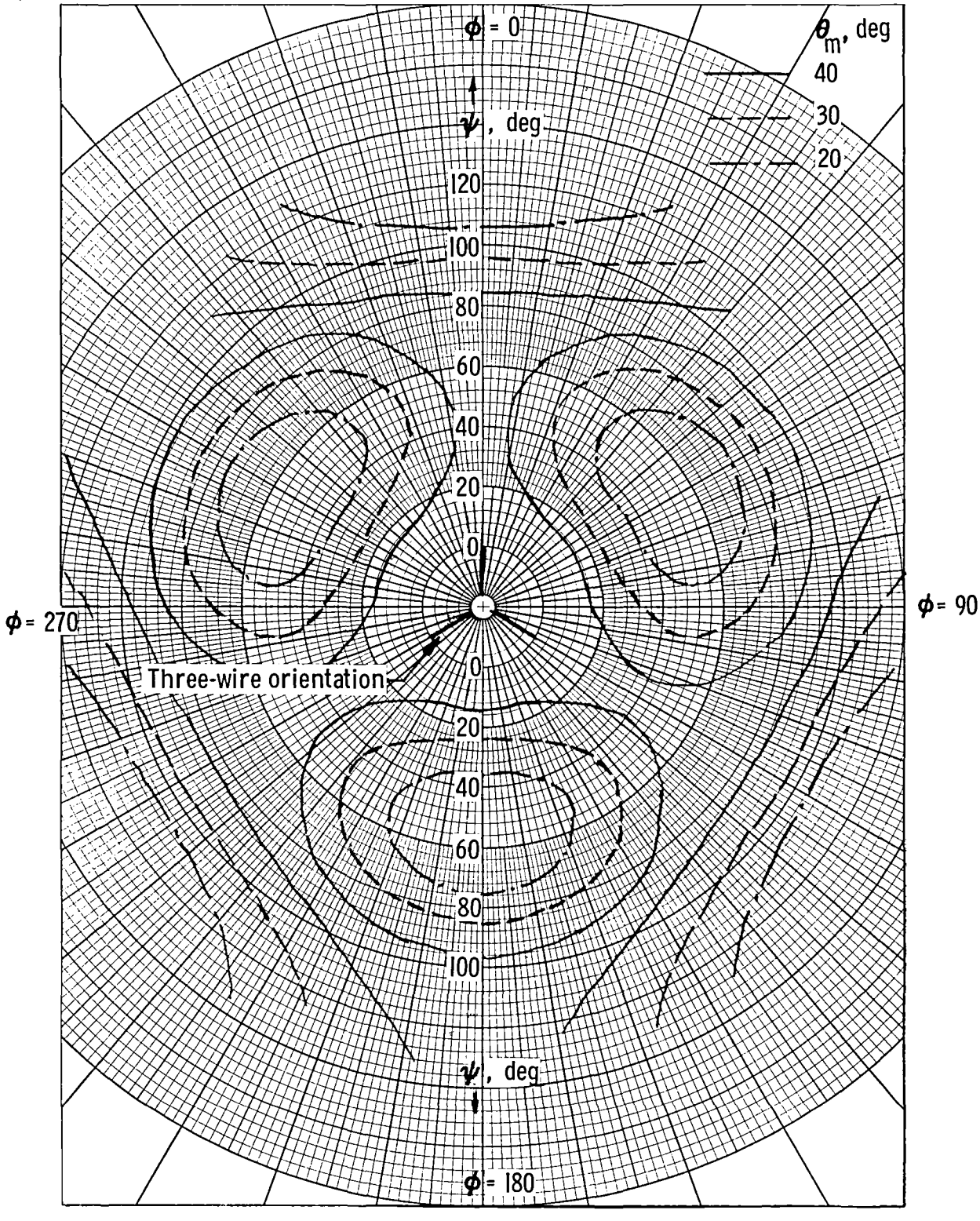

Figure 4.- Minimum angle θ_m with respect to ϕ and ψ. Probe orientation is shown in center of plot.

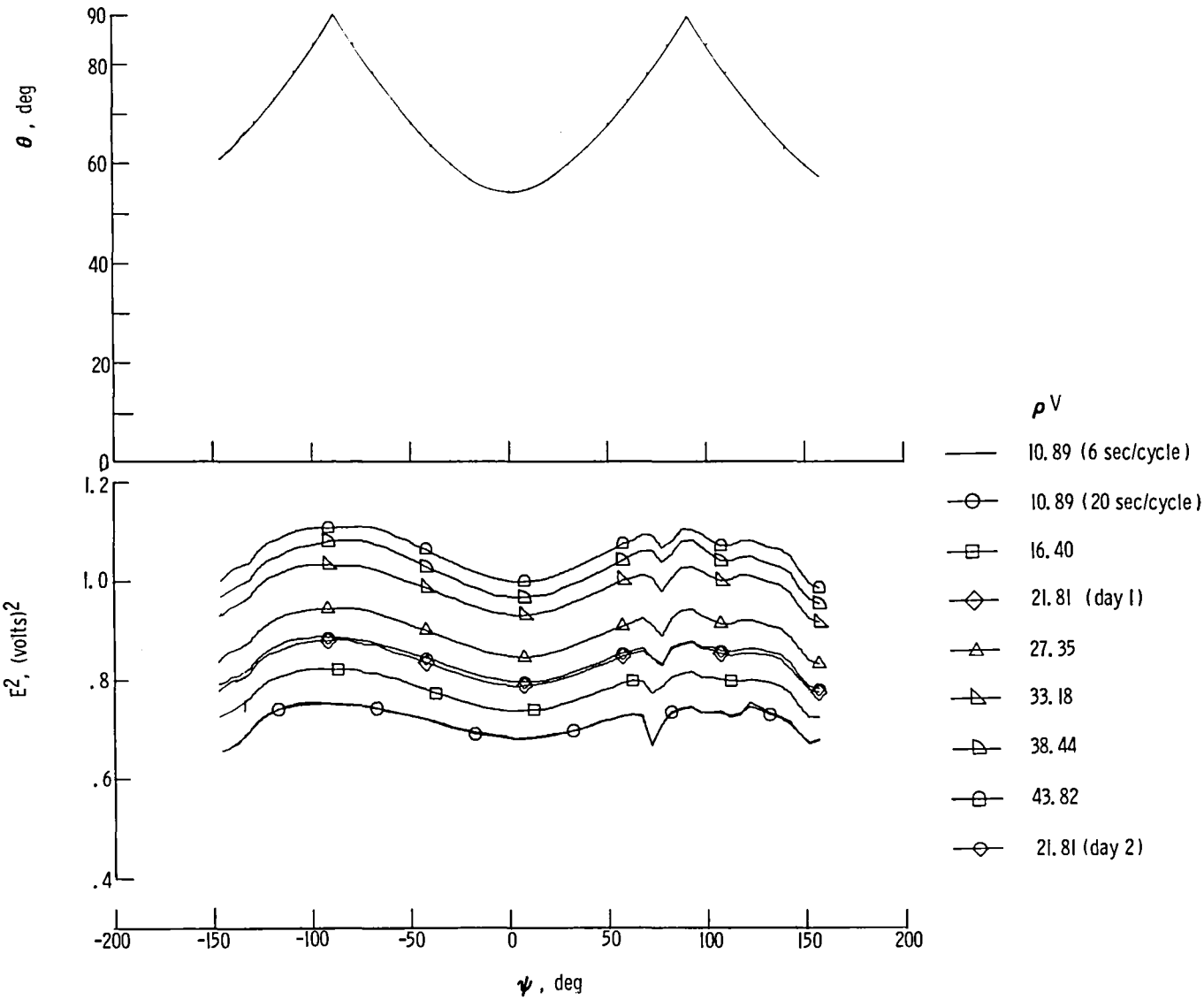

(a) Wire 1.

Figure 5.- Response of a three-wire hot-wire probe for various mass flow rates and probe yaw angles. Wire 1 is aligned vertically. Upper figure displays theoretical angle between mass flow and hot wire.

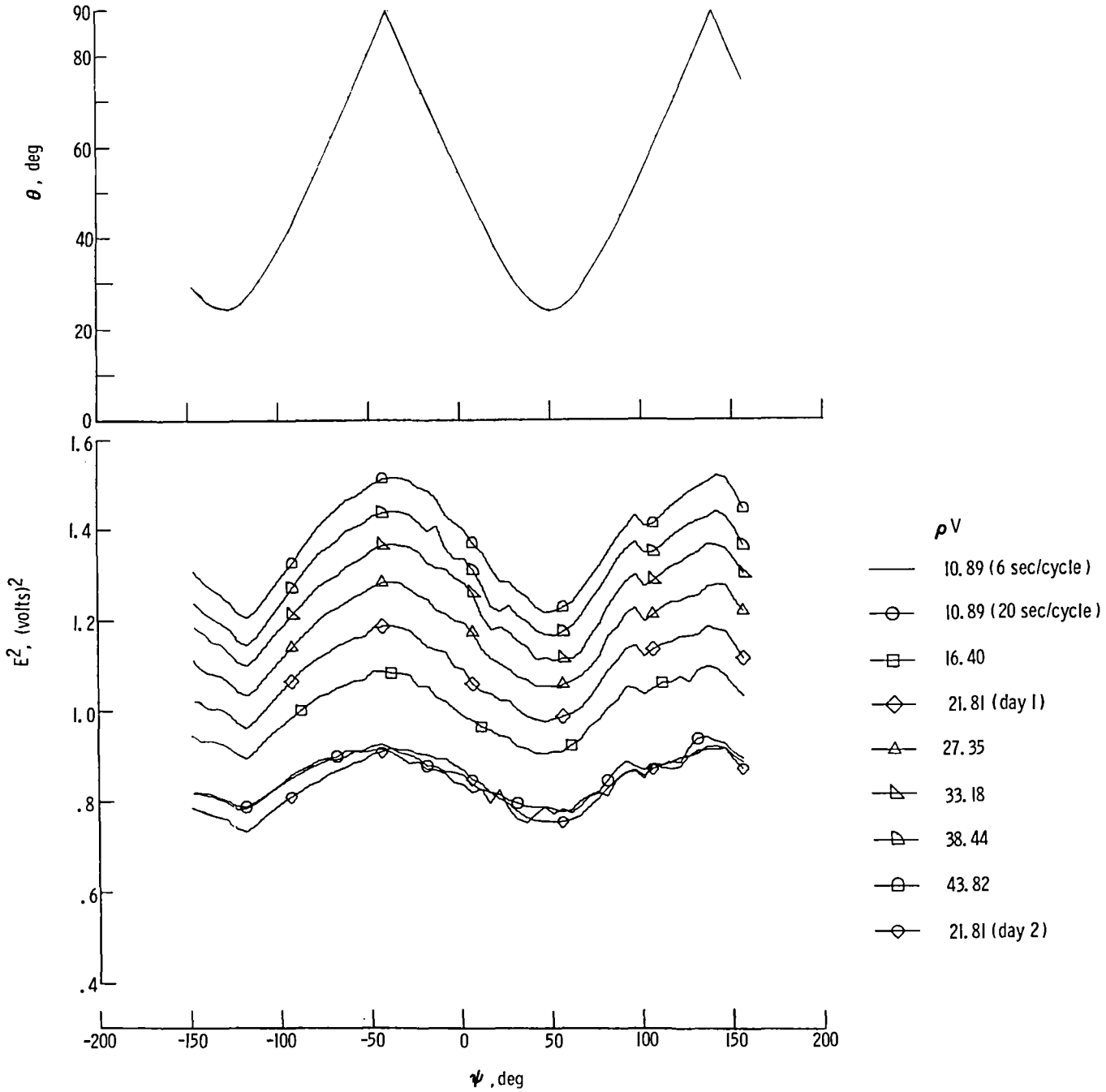

(b) Wire 2.

Figure 5.- Continued.

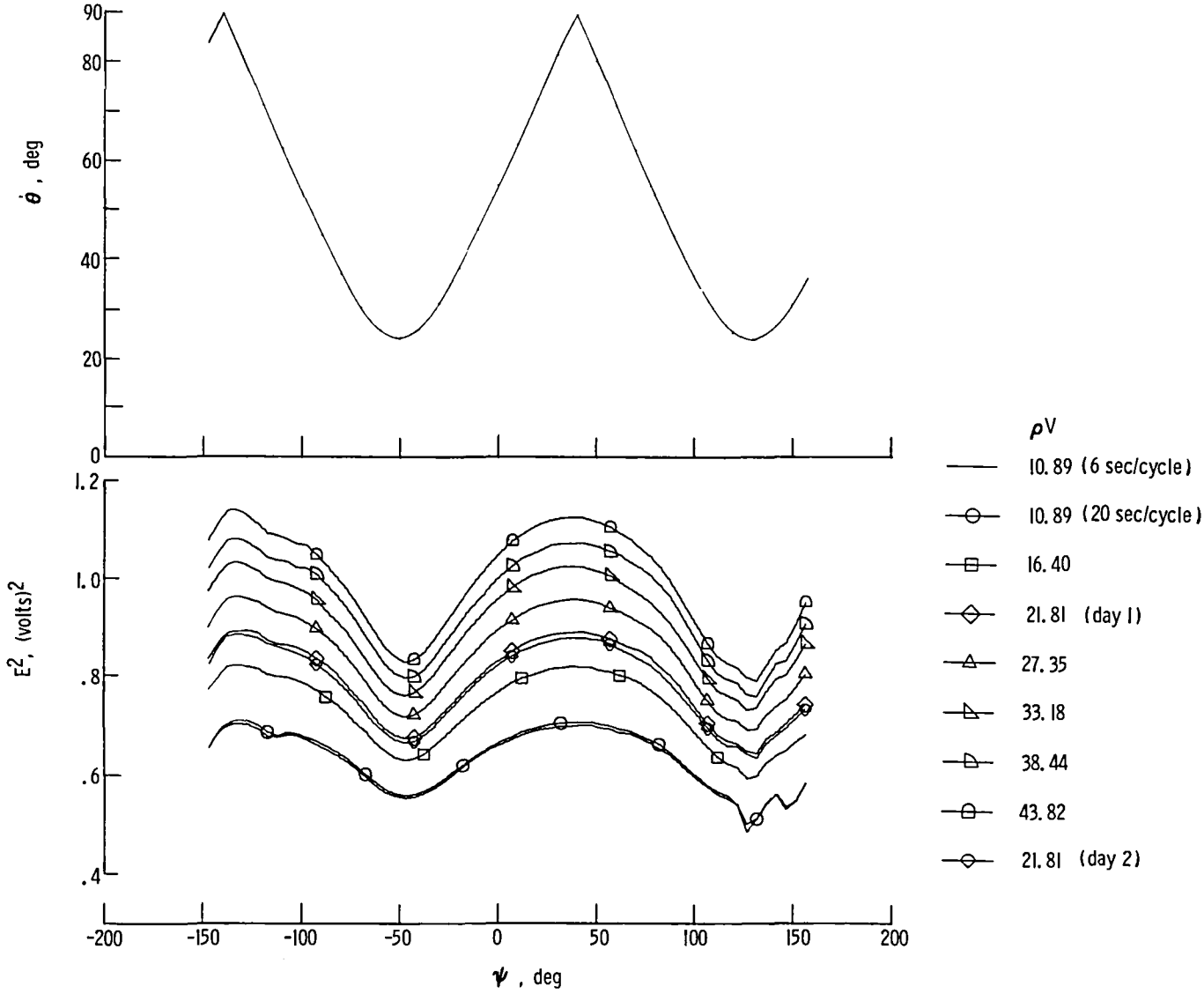

(c) Wire 3.

Figure 5.- Concluded.

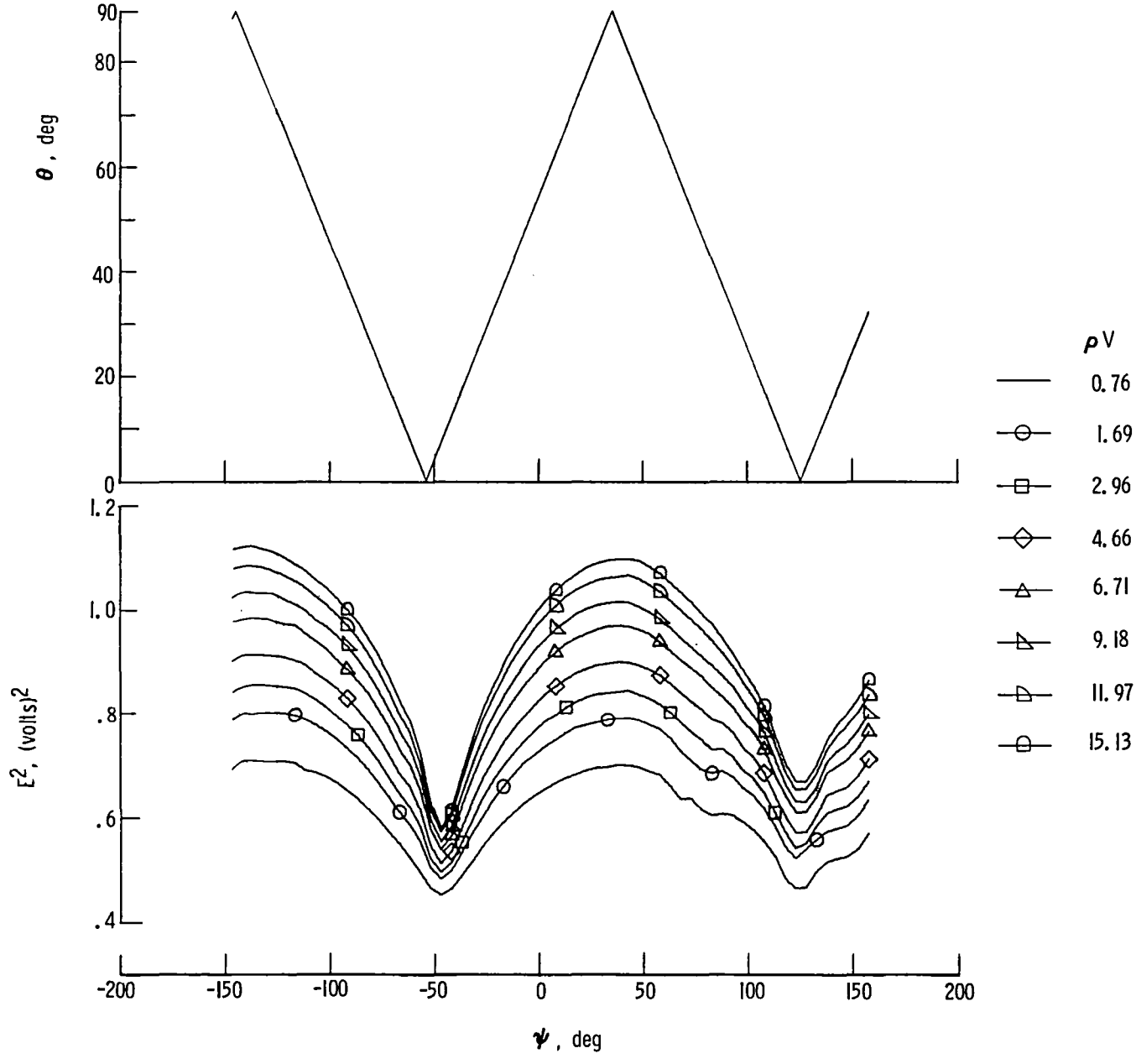

(a) Wire 1.

Figure 6.- Response of a three-wire hot-wire probe for various mass flow rates and probe yaw angles. Wire 1 is aligned horizontally. Upper figure displays theoretical angle between mass flow and hot wire.

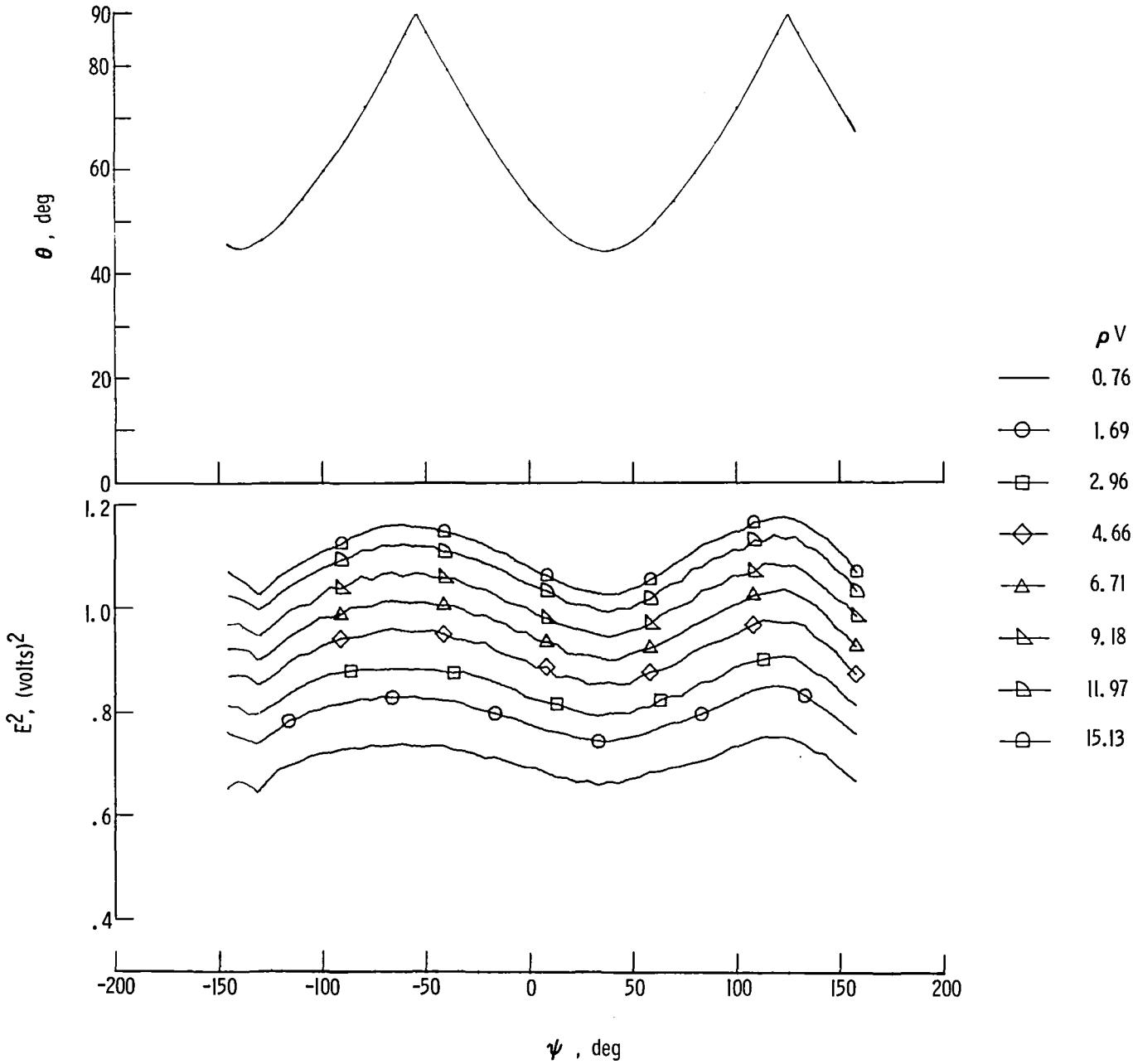

(b) Wire 2.

Figure 6.- Continued.

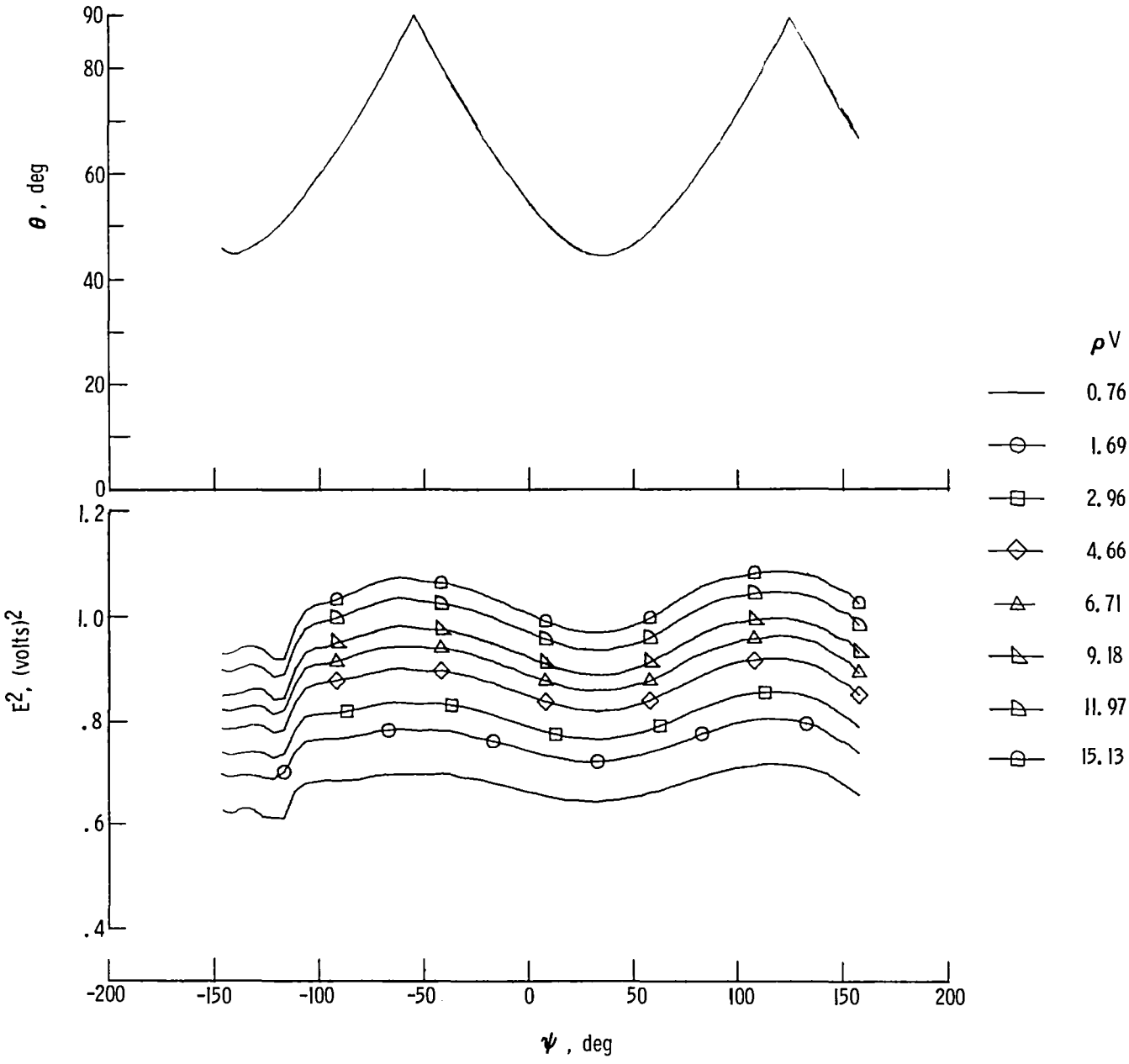

(c) Wire 3.

Figure 6.- Concluded.

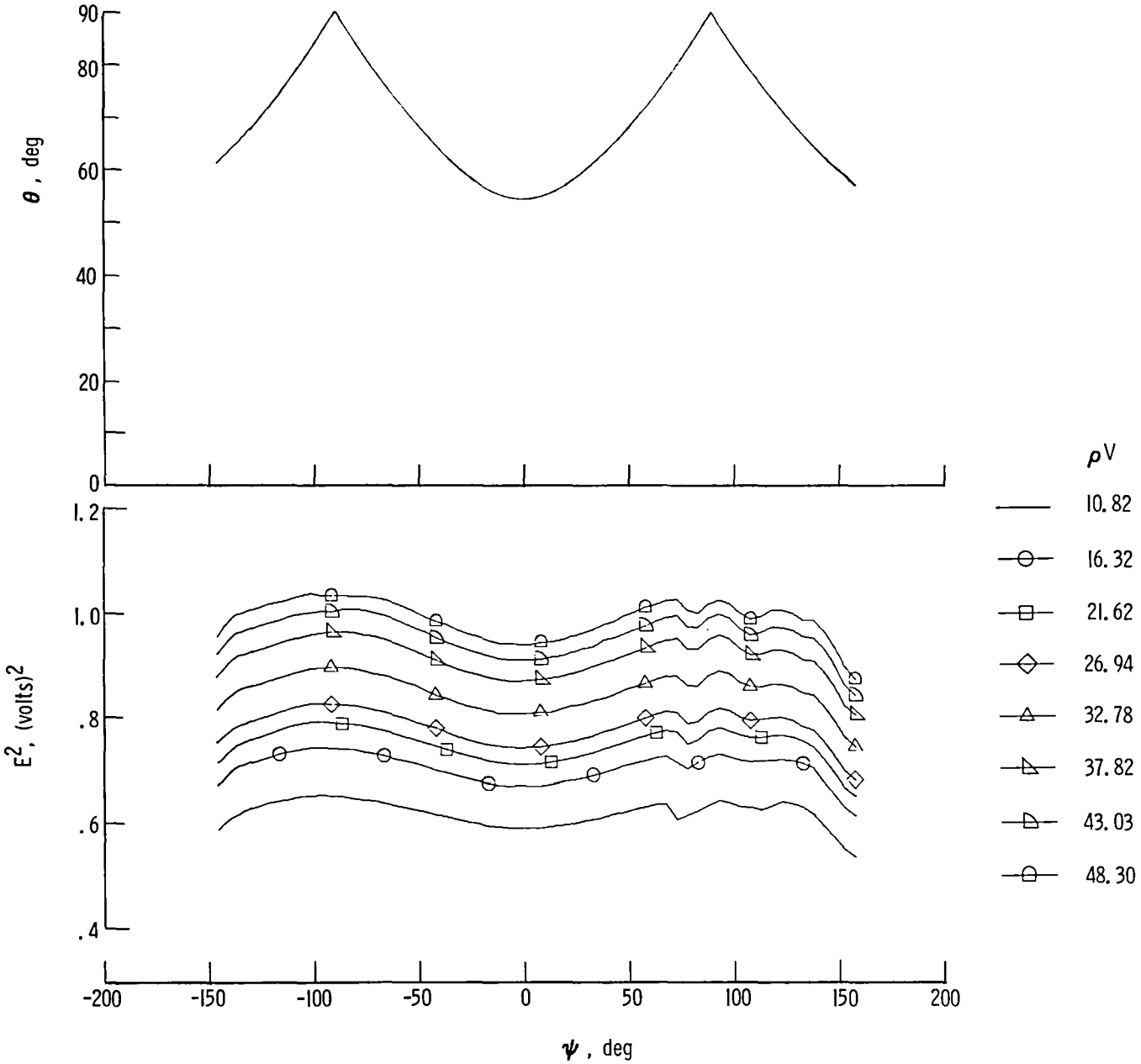

(a) Wire 1.

Figure 7.- Response of a second three-wire hot-wire probe for various mass flow rates and probe yaw angles. Wire 1 is aligned vertically. Upper figure displays theoretical angle between mass flow and hot wire.

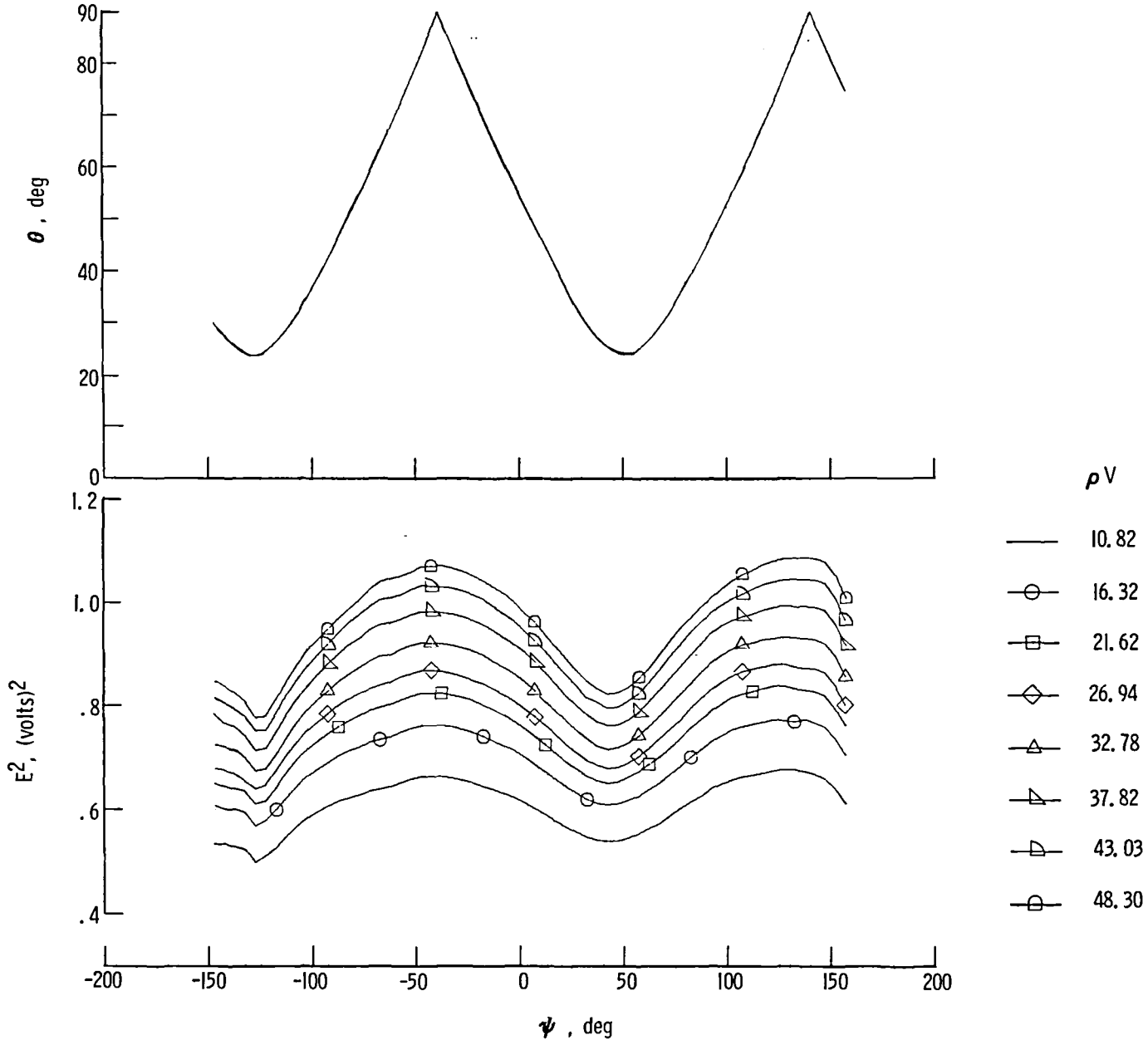

(b) Wire 2.

Figure 7.- Continued.

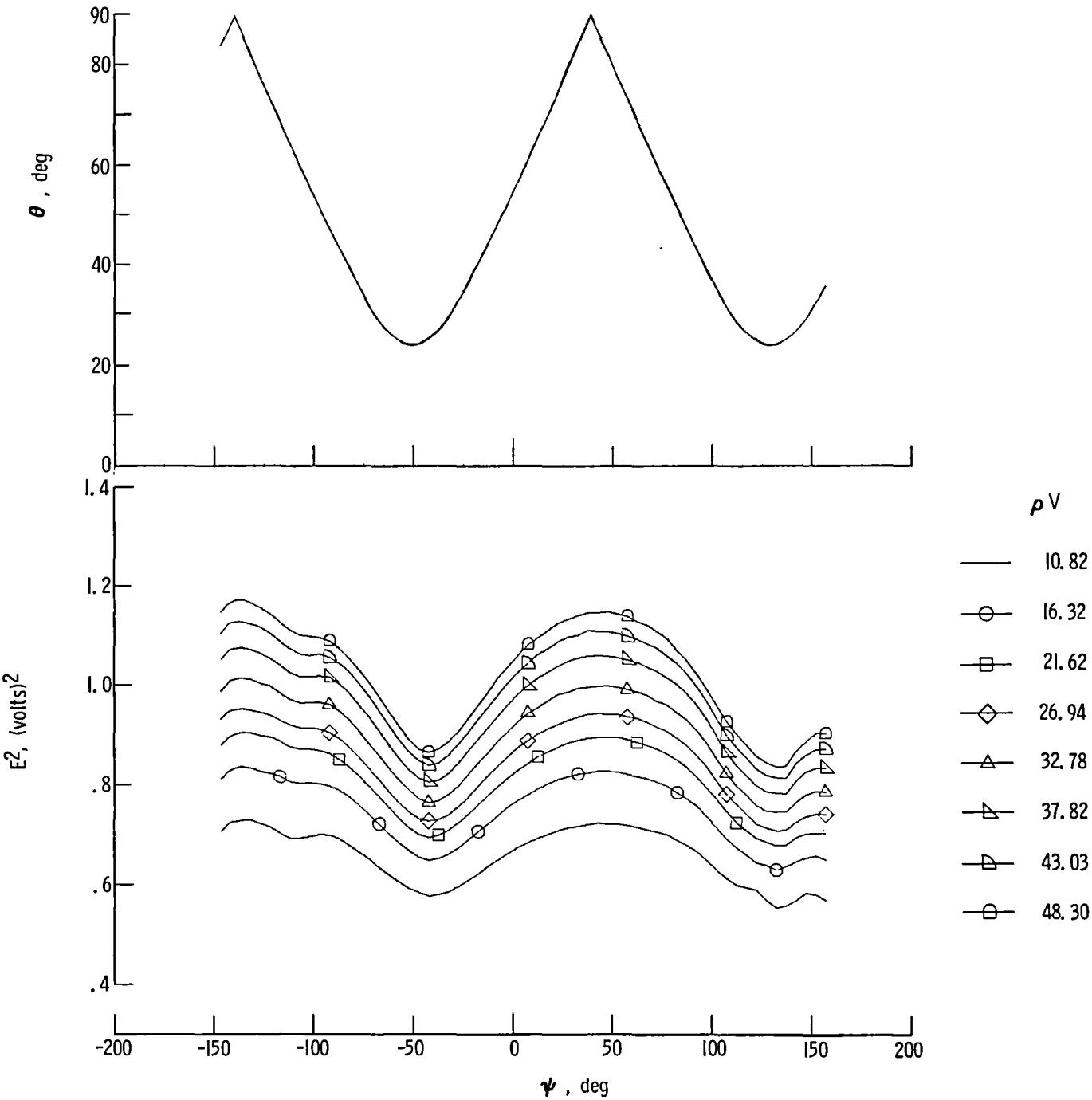

(c) Wire 3.

Figure 7.- Concluded.

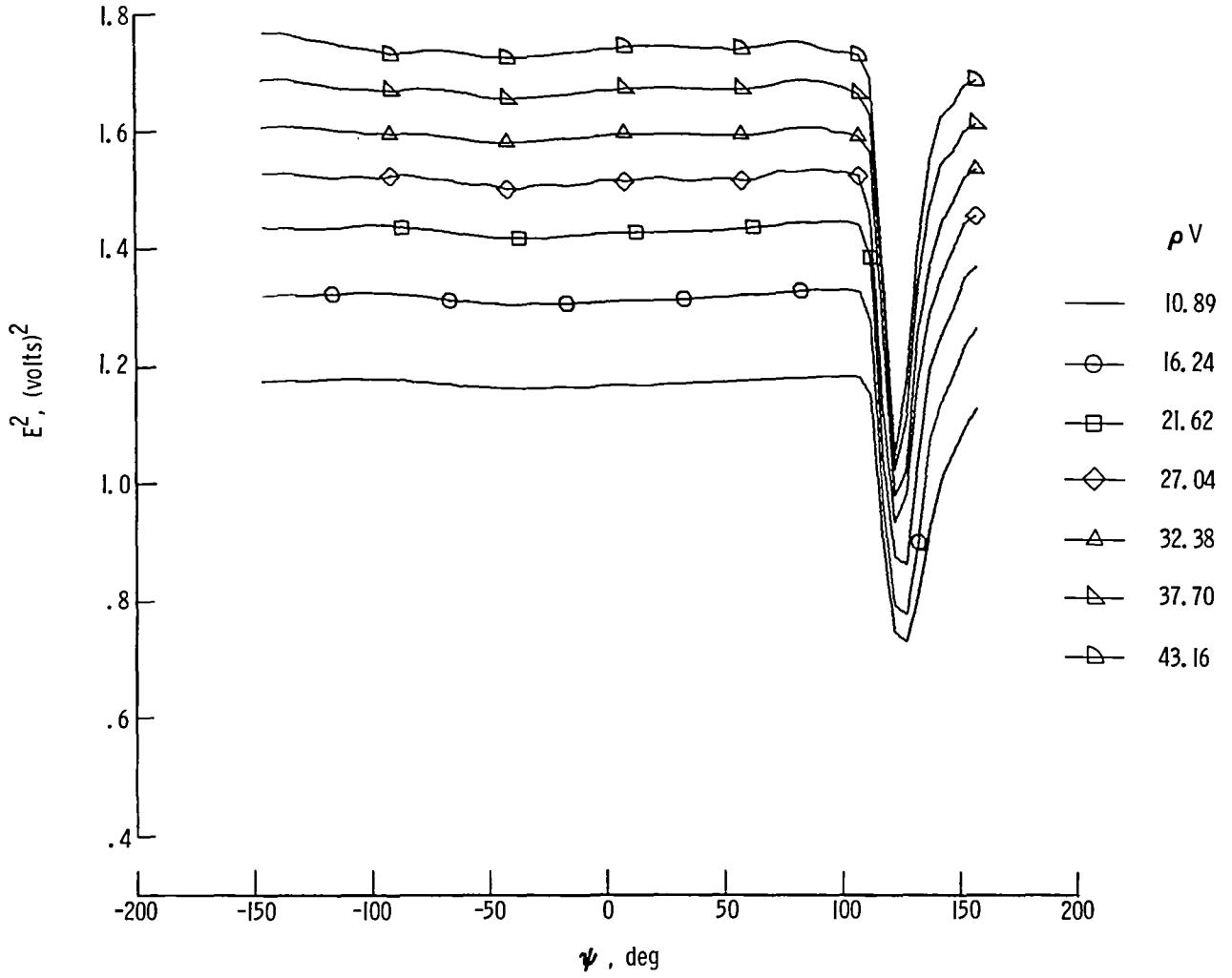

(a) Wire vertical.

Figure 8.- Response of a single-wire hot-wire probe for various mass flow rates and probe yaw angles. The wire was aligned vertically and horizontally. Upper figure in (b) displays the theoretical angle between mass flow and hot wire. (For the wire vertical, θ is constant at 90°.)

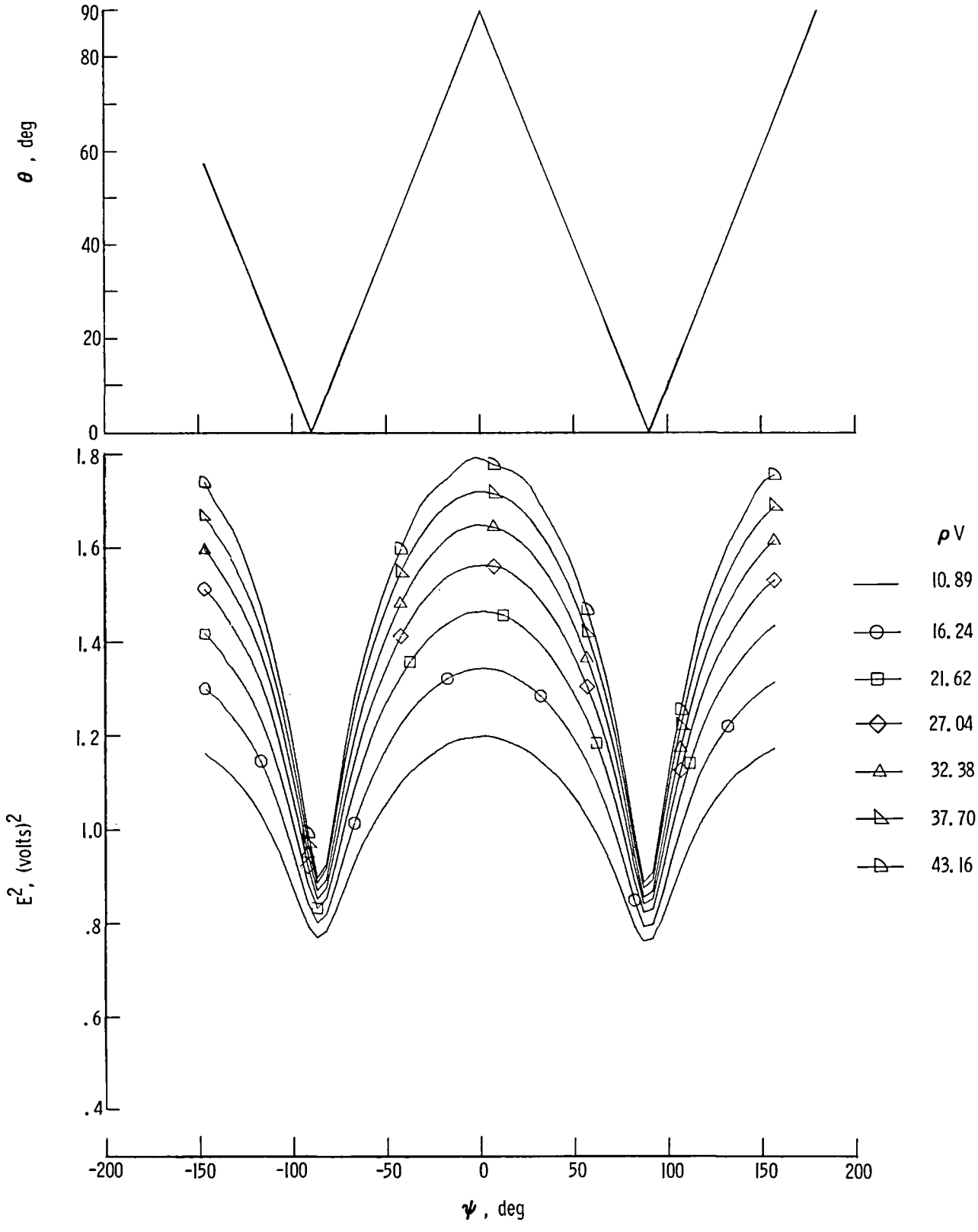

(b) Wire horizontal.

Figure 8.- Concluded.

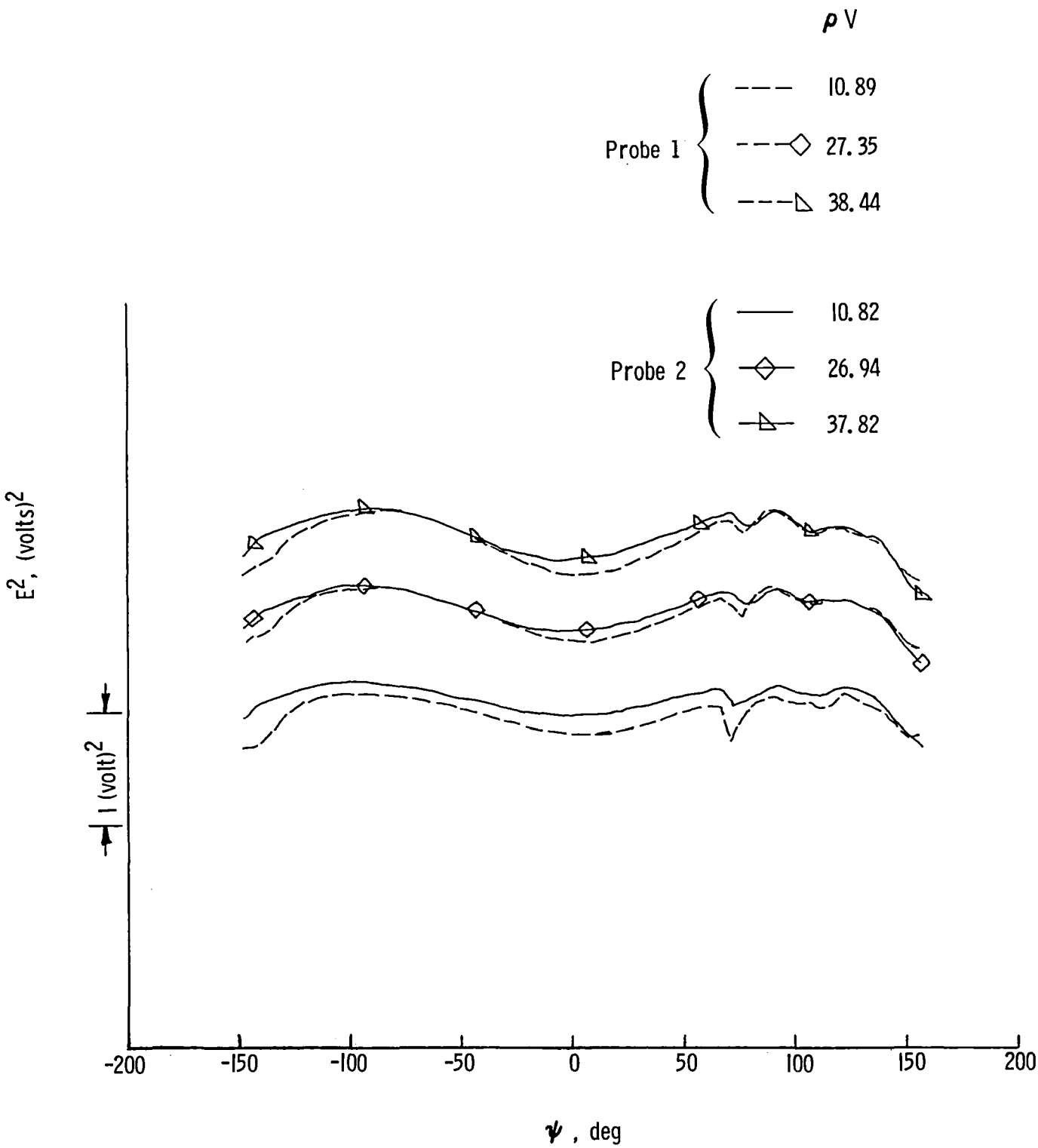

(a) Wire 1.

Figure 9.- Comparison of response for two three-wire hot-wire probes for various mass flow rates and probe yaw angles. Wire 1 is aligned vertically.

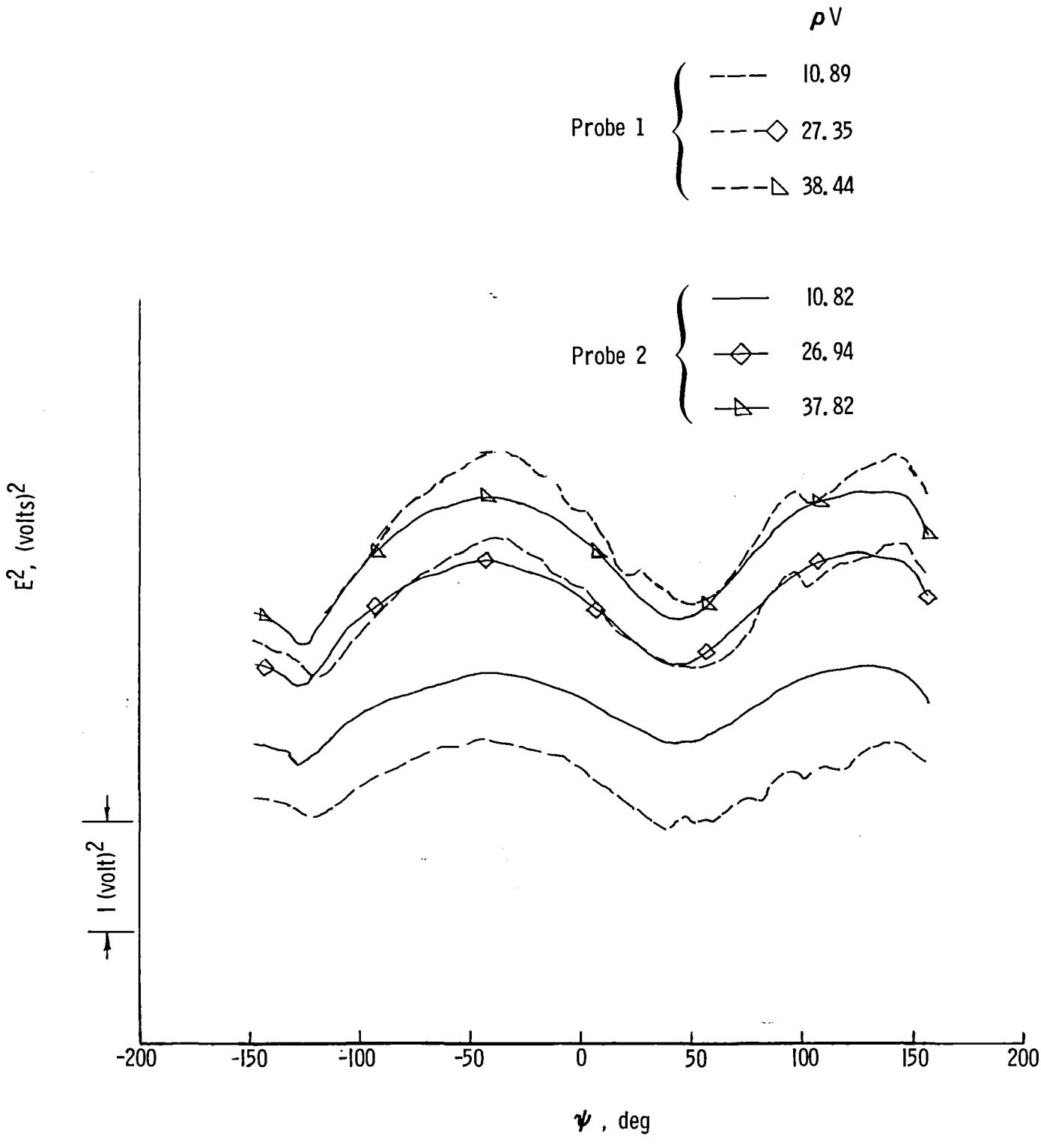

(b) Wire 2.

Figure 9.- Continued.

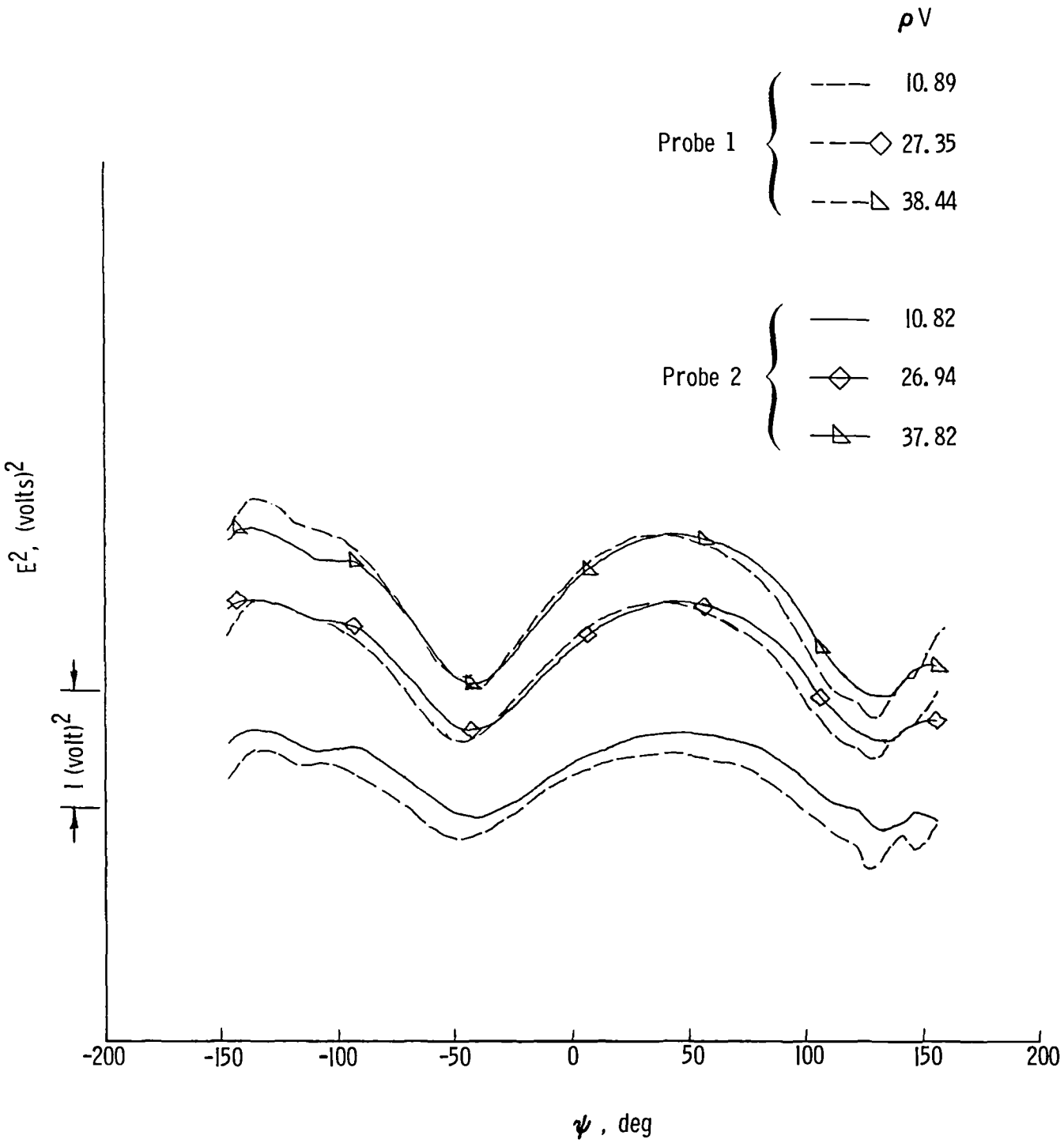

(c) Wire 3.

Figure 9.- Concluded.

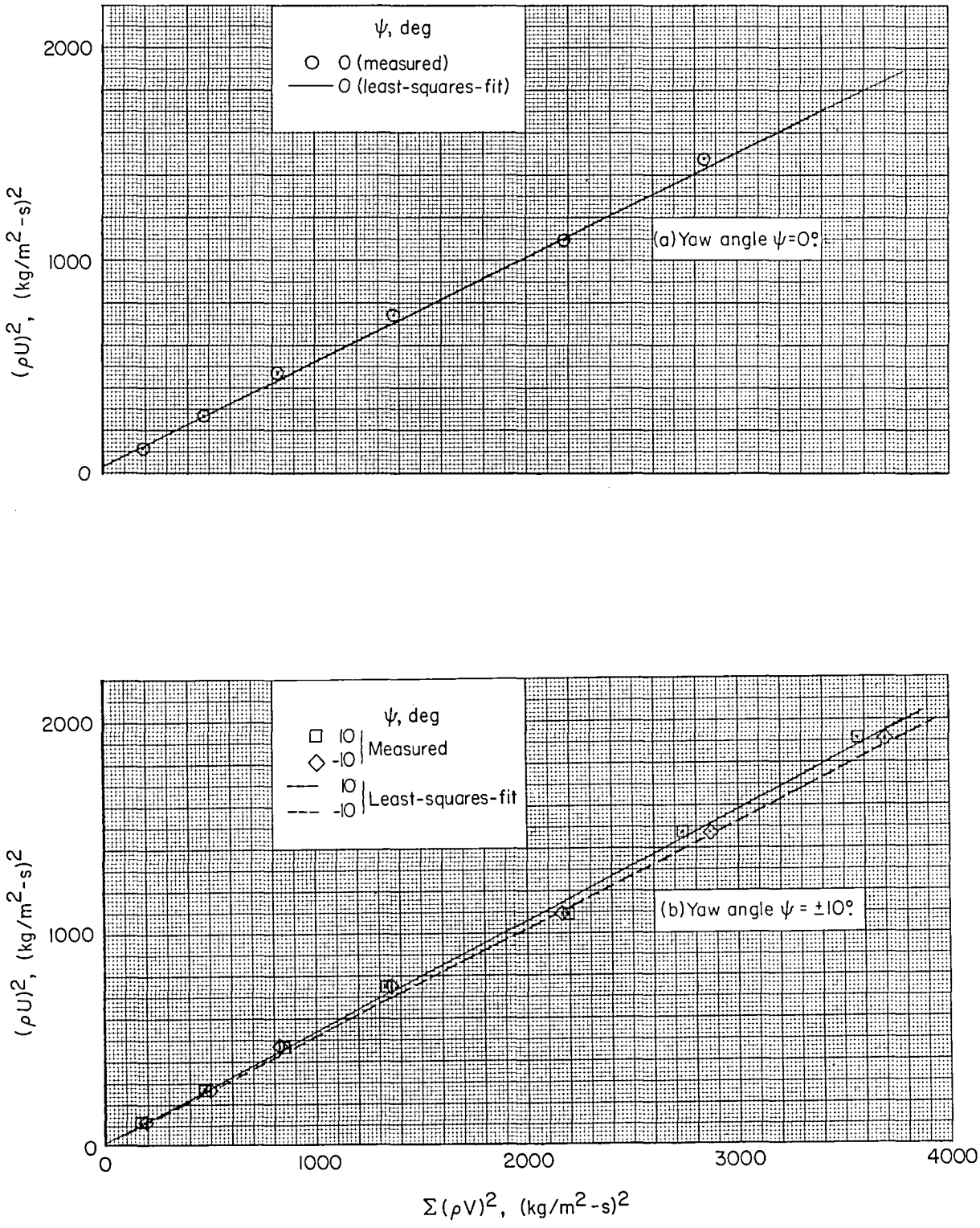

Figure 10.- Comparison of actual mass flow rate (ρU) with flow rate determined from hot-wire probe for different probe flow angles.

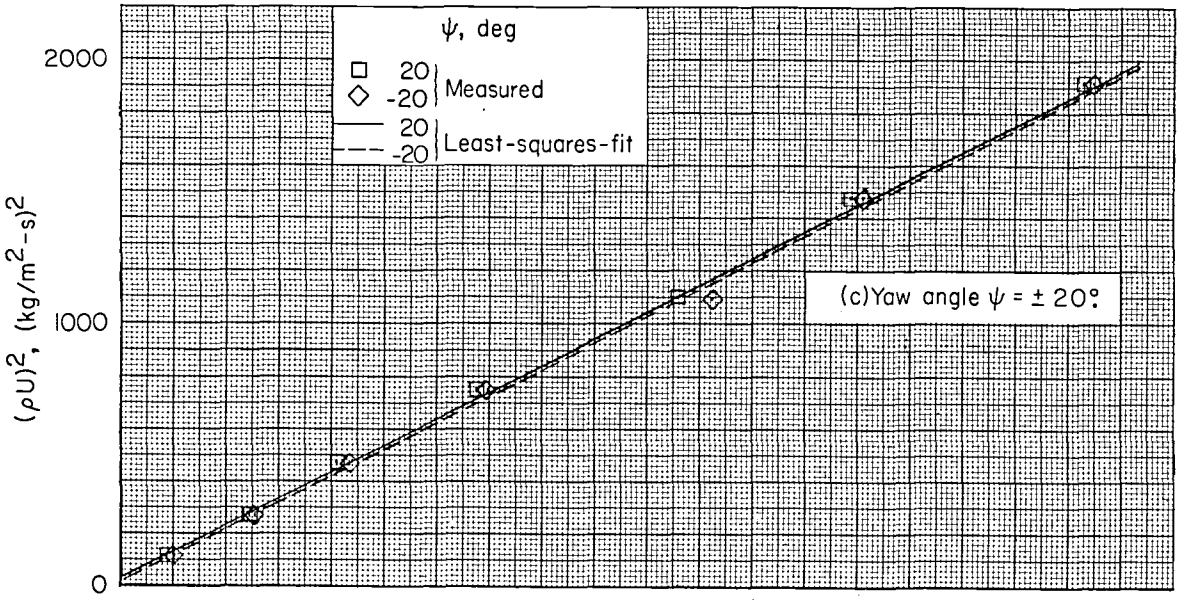

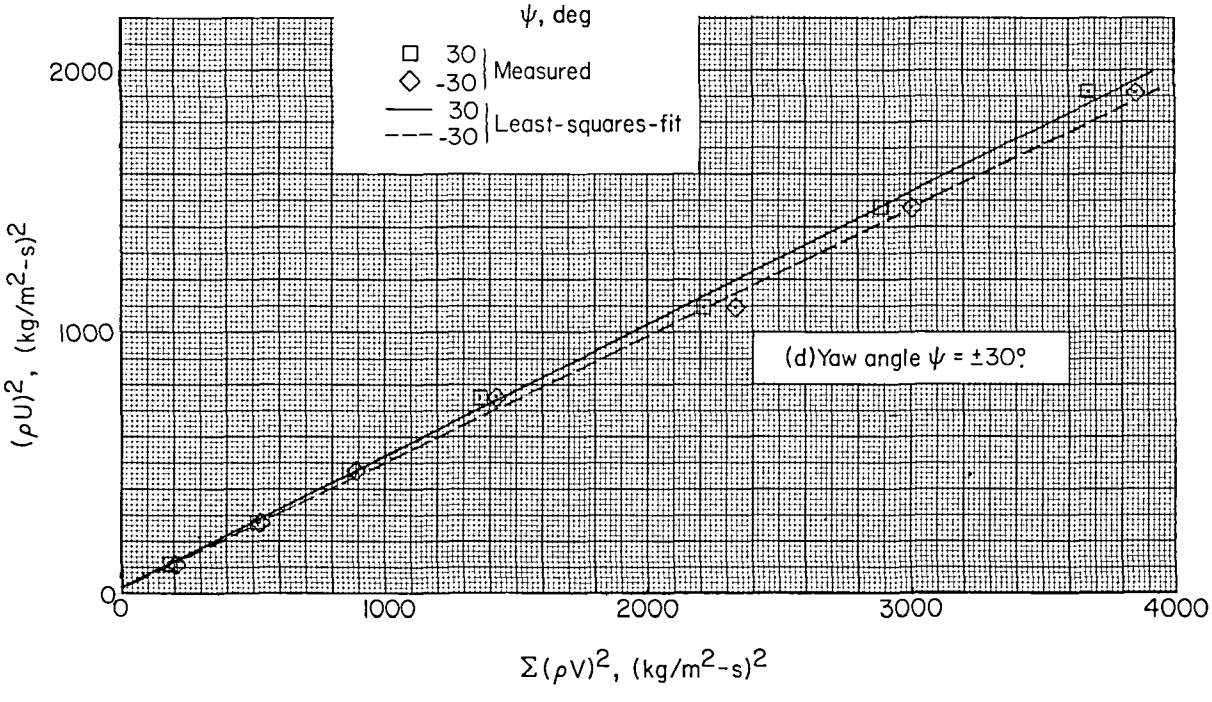

Figure 10.- Concluded.

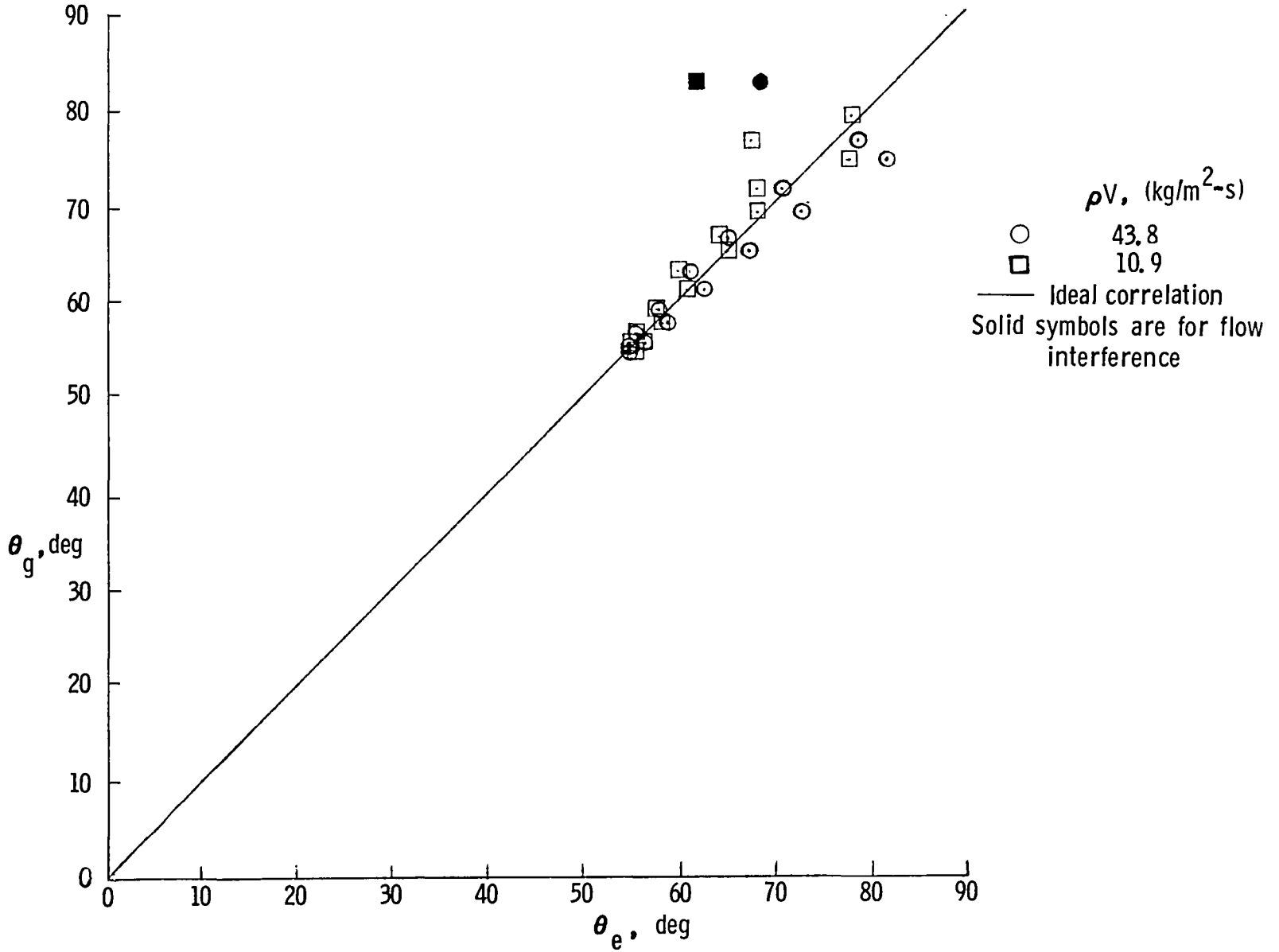

(a) Three-wire probe with wire 1 vertical, data for wire 1.

Figure 11.- Comparison of geometrical angle between mass flow and hot wire and computed flow angle for each of the individual wires of a three-wire probe.

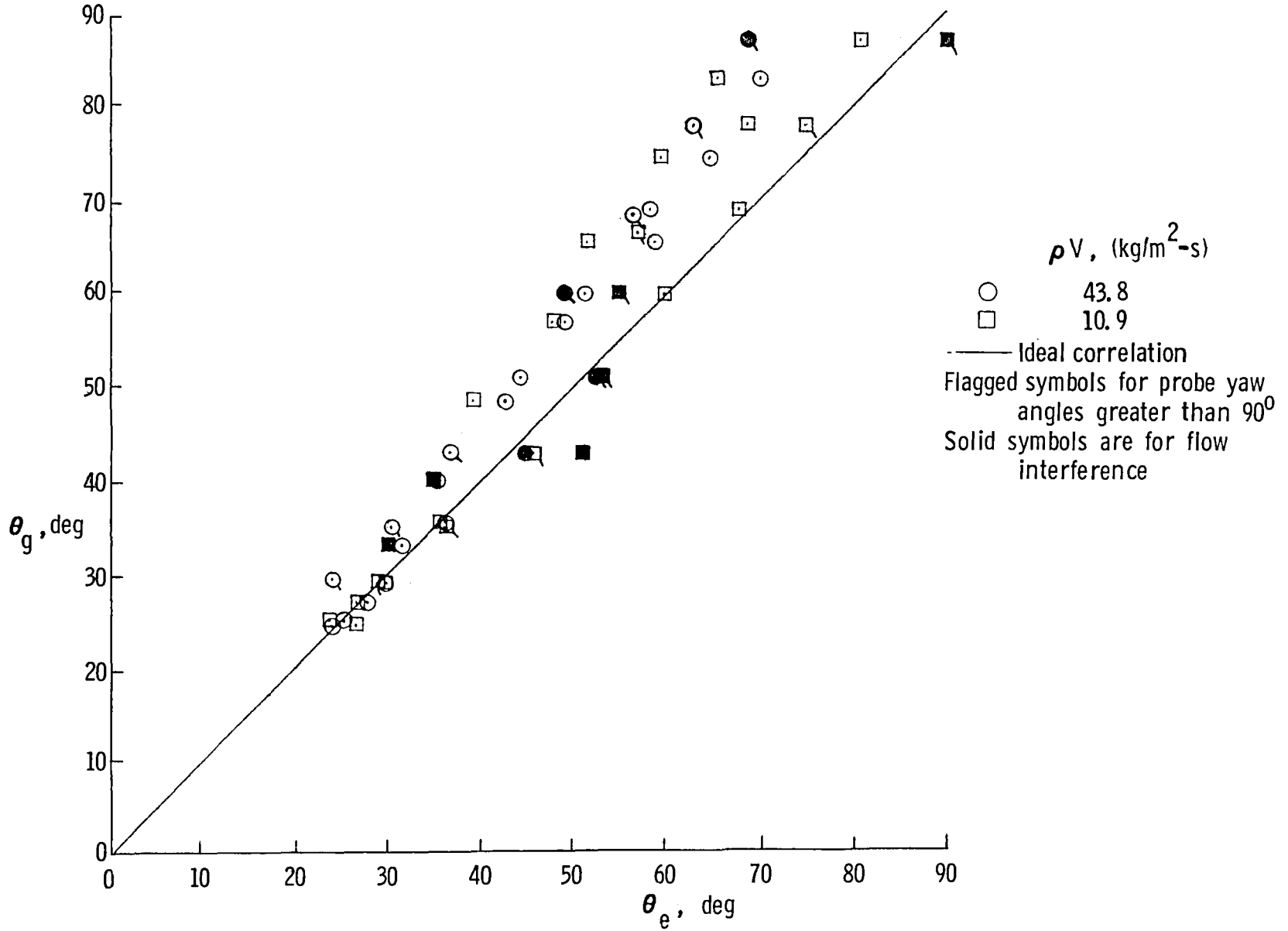

(b) Three-wire probe with wire 1 aligned vertical, data for wire 2.

Figure 11.- Continued.

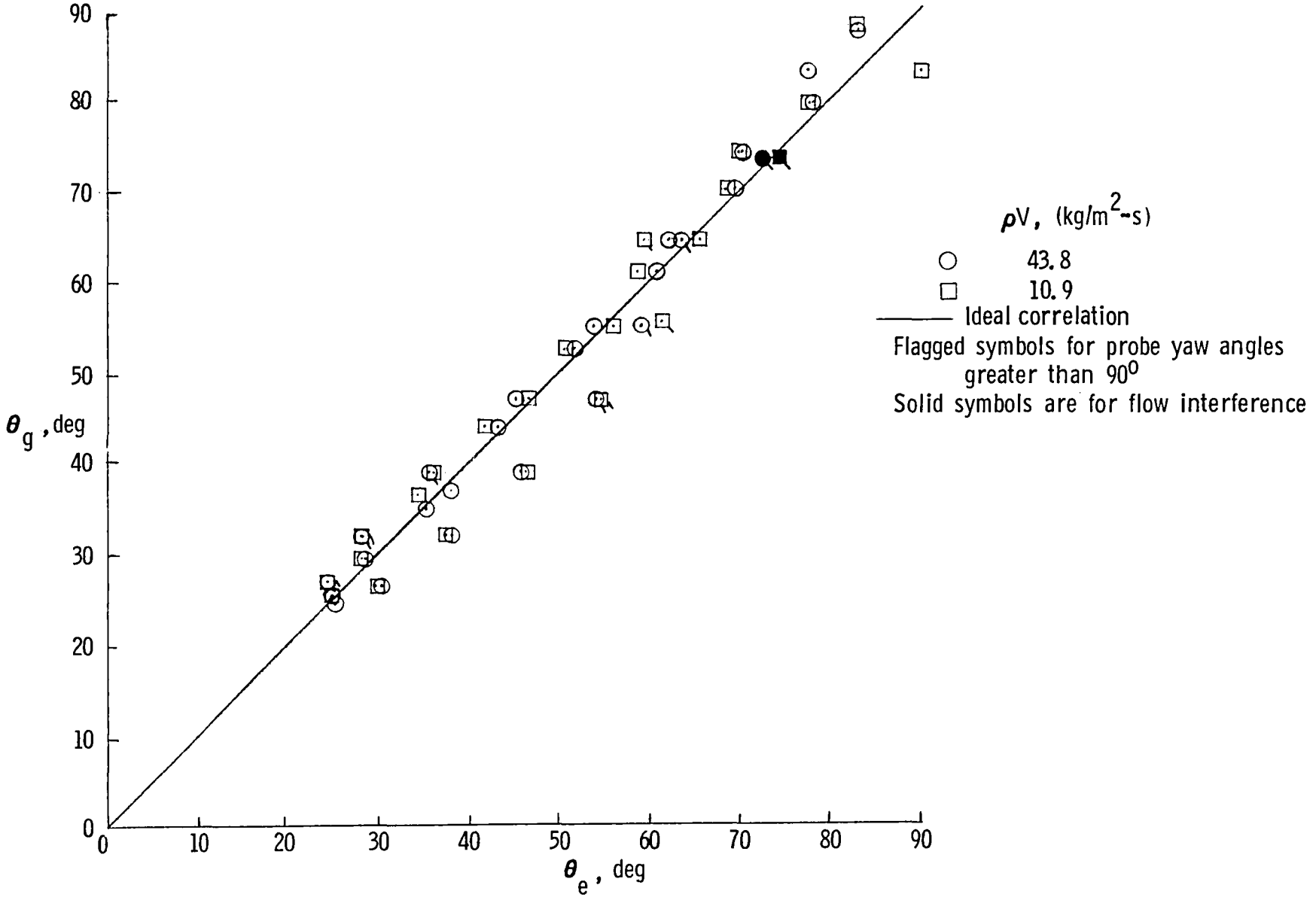

(c) Three-wire probe with wire 1 aligned vertical, data for wire 3.

Figure 11.- Concluded.

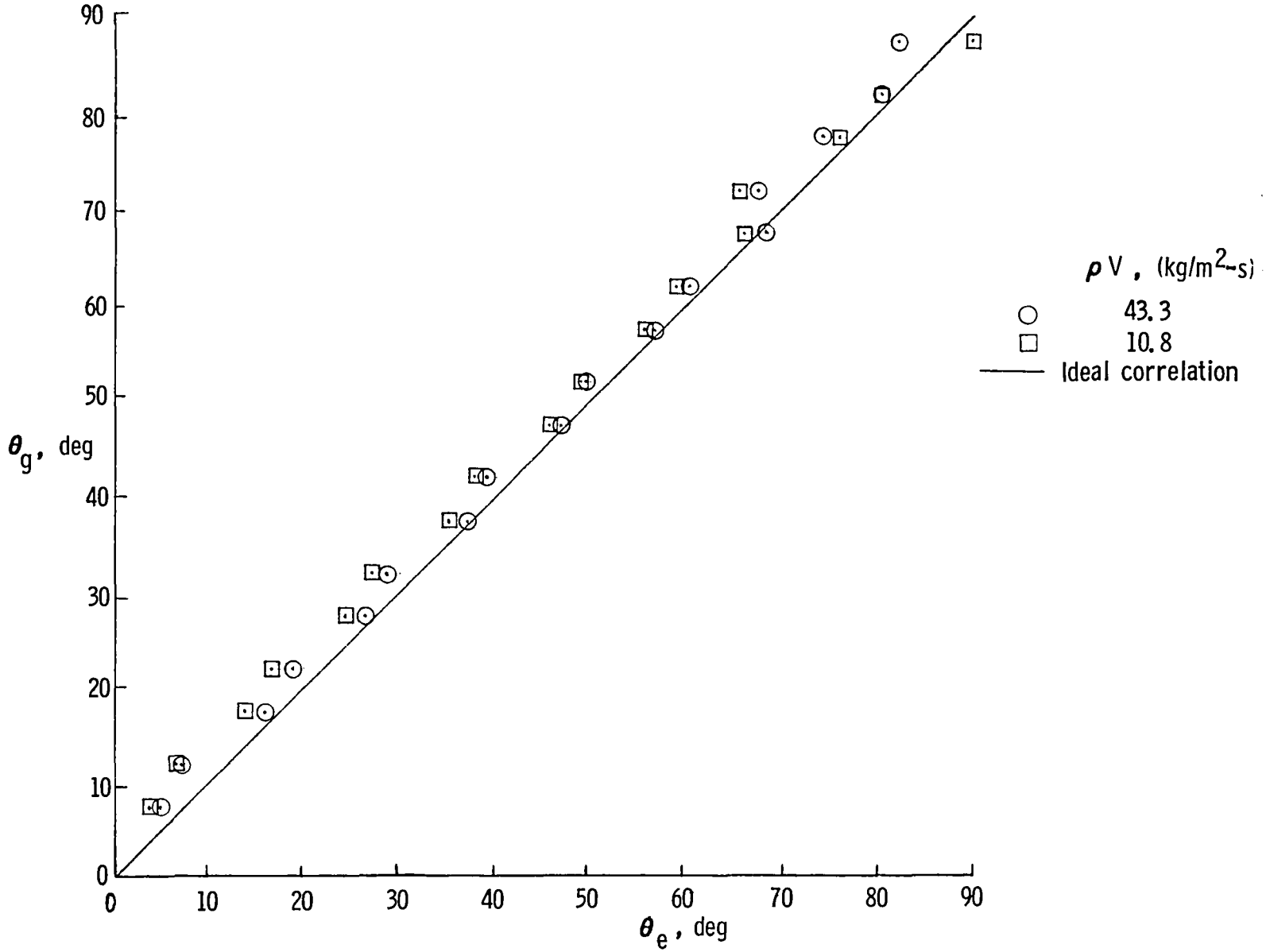

Figure 12.- Comparison of geometrical angle between mass flow and hot wire and computed flow angle for a single-wire probe. Wire horizontal.

1. Report No.	2. Government Accession No.	3. Recipient's Catalog No.
NASA TM-83254		

4. Title and Subtitle	5. Report Date
A CALIBRATION TECHNIQUE FOR A HOT-WIRE-PROBE VECTOR ANEMOMETER	March 1982
	6. Performing Organization Code 505-31-33-09

7. Author(s)	8. Performing Organization Report No.
James Scheiman, Charles Marple, and David S. Vann	L-14445
	10. Work Unit No.

9. Performing Organization Name and Address	11. Contract or Grant No.
NASA Langley Research Center Hampton, VA 23665	
	13. Type of Report and Period Covered Technical Memorandum

12. Sponsoring Agency Name and Address	14. Sponsoring Agency Code
National Aeronautics and Space Administration Washington, DC 20546	

15. Supplementary Notes

16. Abstract

Calibration tests using hot wires were conducted using a newly developed test rig that greatly reduced the data-acquisition time. A comparison of measured and computed velocity-vector magnitude and direction indicates the necessity of complete probe calibration to determine flow interference and/or operating limitation regions. Calibration results indicate that flow rates with 3-percent accuracy and flow angles with 5° accuracy are attainable.

17. Key Words (Suggested by Author(s))	18. Distribution Statement
Hot-wire calibration Three-wire probe Velocity-vector prediction Anemometer	Unclassified - Unlimited Subject Category 35

19. Security Classif. (of this report)	20. Security Classif. (of this page)	21. No. of Pages	22. Price
Unclassified	Unclassified	45	A03

For sale by the National Technical Information Service, Springfield, Virginia 22161

NASA-Langley, 1982

National Aeronautics and
Space Administration

Washington, D.C.
20546

Official Business
Penalty for Private Use, $300

THIRD-CLASS BULK RATE

Postage and Fees Paid
National Aeronautics and
Space Administration
NASA-451

POSTMASTER: If Undeliverable (Section 158 Postal Manual) Do Not Return